CASE FILE COPY

NACA

RESEARCH MEMORANDUM

TRANSONIC LONGITUDINAL AERODYNAMIC CHARACTERISTICS OF A FIGHTER-TYPE AIRPLANE MODEL WITH A LOW-ASPECT-RATIO UNSWEPT WING AND A TEE-TAIL

By Gerald Hieser and Charles F. Reid, Jr.

Langley Aeronautical Laboratory
Langley Field, Va.

NATIONAL ADVISORY COMMITTEE FOR AERONAUTICS

WASHINGTON

October 15, 1956
Declassified July 28, 1960

59

NATIONAL ADVISORY COMMITTEE FOR AERONAUTICS

RESEARCH MEMORANDUM

TRANSONIC LONGITUDINAL AERODYNAMIC CHARACTERISTICS OF A FIGHTER-TYPE AIRPLANE MODEL WITH A LOW-ASPECT-RATIO UNSWEPT WING AND A TEE-TAIL

By Gerald Hieser and Charles F. Reid, Jr.

SUMMARY

The transonic longitudinal aerodynamic characteristics of a fighter-type airplane model have been obtained from tests in the Langley 16-foot transonic tunnel. The results of the investigation provide some general information applicable to the transonic properties of thin, low-aspect-ratio, unswept-wing configurations utilizing a high horizontal tail. The model employs a horizontal tail mounted at the top of the vertical tail and a wing with an aspect ratio of 2.5, a taper ratio of 0.385, and 3.4-percent-thick airfoil sections.

The lift, drag, and static longitudinal pitching moment were measured at Mach numbers from 0.80 to 1.09 and angles of attack from -2.5° to 22.5°. Some of the dynamic longitudinal stability properties of a full-scale airplane have been predicted from the test results. In addition, some visual flow studies on the wing surfaces obtained at Mach numbers of 0.80 and 1.00 are included.

Results of the investigation show that the transonic rise in drag coefficient at zero lift is about 0.030.

At high angles of attack, the model becomes longitudinally unstable at Mach numbers from 0.80 to 0.90, whereas a reduction in static stability is experienced when very high angles of attack are reached at Mach numbers above 0.90.

Longitudinal dynamic stability calculations show that the longitudinal control is good at angles of attack below the unstable break in the static pitching-moment curves, but a typical corrective control applied

after the occurrence of neutral stability has little effect in averting pitch-up.

INTRODUCTION

Airplane designs incorporating thin, low-aspect-ratio, unswept wings represent one type of configuration being considered for supersonic flight and high subsonic cruising speed. It is, therefore, desirable to obtain performance and stability characteristics of an airplane model with these design features at subsonic, transonic, and supersonic Mach numbers. Accordingly, a program has been initiated by the National Advisory Committee for Aeronautics for the purpose of determining the longitudinal and lateral characteristics of a model incorporating a wing with an aspect ratio of 2.5, a taper ratio of 0.385, modified biconvex airfoil sections with a thickness ratio of 0.034, an unswept 0.72-chord line, and 10° negative dihedral. Subsonic performance and stability information and some of the supersonic characteristics are reported in references 1 and 2.

Tests have been conducted in the Langley 16-foot transonic tunnel for the purpose of investigating the transonic longitudinal and lateral characteristics of the model. Results of the lateral investigation are presented in reference 3. The present report includes the longitudinal characteristics of the model both with and without a drooped wing leading edge, wing-tip tanks, dive flaps, and an auxiliary horizontal tail. Tests of the auxiliary tail configuration were included because an earlier investigation of a similar model indicated that a reduction in the horizontal-tail effectiveness occurred at high angles of attack and caused an undesirable longitudinal destabilizing tendency. An analysis of some of the dynamic longitudinal properties based on the present test results, applied to a full-scale airplane similar to the present model, is included herein.

The model was tested at Mach numbers from 0.80 to 1.09 and angles of attack from -2.5° to about 22.5°. The Reynolds number based on wing mean aerodynamic chord varied from 2.8×10^{6} to 3.3×10^{6}.

SYMBOLS

All coefficients are referred to the stability system of axes with the origin on the 0.25-wing mean aerodynamic chord.

C_L lift coefficient, $\frac{\text{Lift}}{qS}$

C_D drag coefficient, $\frac{\text{Drag}}{qS}$

C_m pitching-moment coefficient, $\frac{\text{Pitching moment about mean aerodynamic quarter chord}}{qS\bar{c}}$

q free-stream dynamic pressure, lb/ft^2

S wing area, ft^2

$\bar{c}$ mean aerodynamic chord, $\frac{2}{S}\int_0^{b/2} c^2 dy$, ft

c wing chord at any spanwise station, ft

y lateral distance measured perpendicular to plane of symmetry, ft

b wing span, ft

x longitudinal distance measured from nose of fuselage, ft

x' longitudinal distance measured from wing leading edge, ft

l body length, ft

A cross-sectional area, ft^2

R Reynolds number based on $\bar{c}$

M free-stream Mach number

L/D lift-drag ratio

P_b base pressure coefficient, $\frac{p_b - p_o}{q}$

p_b static pressure at base of fuselage, lb/ft^2

p_o free-stream static pressure, lb/ft^2

m/m_o internal mass-flow ratio

α angle of attack of model (fuselage reference line), deg or radians

α_t effective angle of horizontal tail with respect to the local flow direction, $\frac{C_{m_{tail\ on}} - C_{m_{tail\ off}}}{C_{m_{i_t}}}$, deg

ϵ effective downwash angle at horizontal tail, $\alpha + i_t - \alpha_t$, deg

i_t horizontal tail incidence with respect to fuselage reference line, deg

$C_{m_{i_t}} = \frac{dC_m}{d_{i_t}}$

$C_{L_\alpha} = \frac{dC_L}{d\alpha}$

m' airplane mass, $\frac{\text{Weight}}{g}$, slugs

g acceleration due to gravity, ft/sec^2

l_t tail length, longitudinal distance between 0.25-wing mean aerodynamic chord and 0.25-tail mean aerodynamic chord, ft

ρ density of air, slugs/ft^3

V free-stream velocity, ft/sec

$T_{1/2}$ time to damp longitudinal oscillation to 1/2 amplitude, sec

t time, sec

θ angle between airplane reference axis and the horizontal, radians

ν dynamic-response parameter, $\frac{\rho V_1^2 S\bar{c}}{2I_y}$, radians/sec^2

V_1 initial velocity upon entering maneuver, ft/sec

I_y longitudinal moment of inertia about center of gravity, slug-ft^2

τ time factor, $\frac{m'}{\rho S V_1}$, sec

$C_{m_{\dot{\alpha}}}$ damping derivative, $\frac{\partial C_m}{\partial \dot{\alpha}\bar{c}/2V}$

$C_{m_{\dot{\theta}}}$ damping derivative, $\frac{\partial C_m}{\partial \dot{\theta}\bar{c}/2V}$

K_y dimensionless radius of gyration, $\sqrt{I_y/m'\bar{c}^2}$

Differentiation with respect to time is designated by means of a dot or double dots above the dependent variable.

DESIGNATION OF COMPONENTS

The configurations are designated by use of the following symbols:

W wing

N drooped leading edge

F fuselage and canopy

V vertical tail and dorsal fin

H horizontal tail (subscript designates tail incidence in degrees)

E modified afterbody with inlet ducts faired

E_1 modified afterbody with inlet ducts open and low internal flow

E_2 modified afterbody with inlet ducts open and high internal flow

D_1 dive flaps on side of fuselage (number following denotes deflection angle in degrees)

D_2 dive flaps beneath fuselage (number following designates deflection angle in degrees)

D_3 dive flaps beneath fuselage with shell deflector added (number following denotes deflection angle in degrees)

H_A auxiliary horizontal tail at $i_t = -2.5^\circ$

T wing tip tanks

MODEL AND APPARATUS

Model

The model has a cast aluminum-alloy fuselage and a machined steel wing and tail assembly. A three-view sketch of the basic model including principal dimensions is presented as figure 1(a), and photographs of the model and sting-support system are shown in figure 2. The axial distribution of the cross-sectional area is shown in figure 3.

The wing has no geometric twist or incidence but has 10° negative dihedral. For most configurations tested, the forward 15 percent of the wing was drooped 3°.

The model was tested with and without internal air flow. For tests without air flow, the duct inlets were replaced with metal fairings as shown in figure 1(b). For tests with flow, the air-flow quantity through the model was adjusted by the installation of one of two different wire-mesh throttling screens in the air ducting system. In order to provide a sufficiently large jet exit, the internal air flow was ducted through a modified afterbody passage installed beneath the fuselage as shown in figures 1(b) and 2(a) to 2(d).

In addition to tests of the basic configuration, the model was tested with wing-tip tanks, dive flaps, and an auxiliary horizontal tail. (See figs. 1(b) and 2(b) to 2(e).) Table I gives a list of the various configurations tested.

The tip tanks have a circular cross section, 1.716 inches maximum diameter, a fineness ratio of 12.1, and were mounted symmetrically with respect to the wing chord plane.

Two different dive-flap configurations were tested; one consisted of two flaps (D_1), one opening outward from each side of the fuselage at the 78.7-percent fuselage station, whereas the other consisted of

two flaps (D_2) located at the 52-percent fuselage station mounted 30° up from the plane of symmetry. For both configurations, the area of each flap is 0.0341 square foot, and the deflection from the closed position was 60° for the flaps mounted at the 52-percent fuselage station and both 30° and 60° for the flaps mounted on the side of the fuselage. For one group of runs with the flaps at the 52-percent fuselage station, a small shell deflector was placed ahead of each flap as would be required on a full-scale airplane to protect the flaps from ejected cartridges.

The auxiliary horizontal tail was mounted on the fuselage reference line at 2.5° negative incidence. The exposed area of this tail is one-half the area of the main horizontal tail, and the taper ratio of the exposed panel is 0.284.

Apparatus

The tests were conducted in the Langley 16-foot transonic tunnel which has an octagonal slotted throat permitting a continuous speed variation to Mach numbers slightly greater than 1.00. A complete description of the tunnel is given in reference 4.

The sting-support system, described in reference 5, is designed so that the model is located near the tunnel center line at all angles of attack.

Forces and moments were measured by use of a six-component strain-gage balance. Two static-pressure orifices were located in the rear of the model for measurement of base pressures. A rake consisting of 2 static orifices and 14 total-pressure tubes was installed in the plane of the jet exit to determine the internal mass flow when the inlet ducts were open.

TESTS AND ACCURACY

Tests

Simultaneous measurements of forces and moments were obtained for the various configurations listed in table I. The Mach number and angle-of-attack ranges covered by the tests are given in table I and the variation of test Reynolds number, based on wing mean aerodynamic chord, is shown in figure 4.

Corrections and Accuracy

The Mach number in the test region is believed to be accurate to ±0.005 (ref. 4). An adjustment to the model angle of attack for airstream misalinement was determined from tests of the model upright and inverted. The angle of attack was also corrected for sting and balance deflections and is estimated to be accurate to $\pm 0.1^{\circ}$.

The model chordwise force was adjusted to the condition of free-stream static pressure at the model base. The drag-coefficient data were corrected for the internal-flow drag for the tests conducted with internal flow. A correction to the pitching-moment coefficients was applied to account for the reaction to the change in momentum of the internal air flow in the model ducting system as a result of the modified afterbody.

No attempt has been made to adjust the data for the effects of sting interference or model aeroelasticity.

The data at the low supersonic Mach numbers are affected somewhat by boundary reflected disturbances impinging on the model. It has been estimated that the present model in the Langley 16-foot transonic tunnel should be free of all such disturbances at Mach numbers above about 1.07.

On the basis of balance accuracy and repeatability of the data, the aerodynamic coefficients are estimated to be accurate to the following limits:

$$C_L = \pm 0.005 \qquad C_D = \pm 0.0005 \qquad C_m = \pm 0.002$$

RESULTS

A list of the various configurations tested is presented in table I. Lift, drag, and pitching-moment data for each of these configurations are presented in figures 5 to 19. The variation of mass-flow ratio with angle of attack and Mach number is presented in figure 20 for the model with the two different duct throttling screens. The higher mass-flow ratio approximates the requirement of a comparable airplane in level flight. The base pressure coefficients given in figure 21 for the basic configuration are included for the purpose of showing the effect of angle of attack and Mach number on base pressure. Addition of the modified afterbody and variation in mass-flow ratio also influenced the magnitude of the base pressures. These effects are shown in figure 21 by some typical curves at 0.8 Mach number.

Corrections to the lift, drag, and pitching-moment results for the effects of the modified afterbody were determined from the data obtained

during tests of the model with no internal air flow with and without the afterbody modification. These corrections were determined for the model with the horizontal tail at zero incidence and, therefore, have been applied only to the results contained in the analysis figures (figs. 22 to 33) where data for this configuration were utilized.

DISCUSSION

Performance Data

Basic model.- The effect of Mach number on drag coefficient at constant values of lift coefficient is given in figure 22 for the complete model with high mass flow through the ducts and the wing leading edge drooped 3°. These data are corrected for the effects of the modified afterbody. The dashed portions of the curves are estimated fairings based on the data and considerations of wind-tunnel-wall reflected disturbances and model support interferences. The zero-lift transonic rise in drag coefficient for the complete model is about 0.030 as compared with the value of about 0.016 for a research model employing a thin, low-aspect-ratio, unswept wing and a body of revolution with no tail surfaces (ref. 6). Inspection of the data from the present tests (see figs. 5 and 6) indicates that the horizontal and vertical tail of the present model contribute about half this difference in drag rise, whereas at least part of the other half can probably be attributed to the difference in the longitudinal distribution of cross-sectional area existing between the two models. It is, therefore, possible that some reduction in drag rise might be realized by application of the concepts of area distribution as outlined in reference 7. However, the performance gains which would be realized by a reduction in the drag-rise coefficient would probably not be very large because of the small airplane wing area.

Increasing the lift coefficient from 0 to 0.40 at subsonic speeds increases the drag coefficient from about 0.014 to about 0.040 (fig. 22). This increase in drag is commensurate with that obtained for the wing and body combination of reference 6.

The slight decrease in drag coefficient noted at a Mach number of about 0.90 (fig. 22) is probably associated with the location of the main wing shock. As pointed out in reference 8, the main wing shock moves rearward with increasing Mach number, and a slight drag reduction may exist when the shock is in the vicinity of the wing maximum thickness.

The variation of lift coefficient with angle of attack for the basic model (figs. 5, 11, and 12) shows that the lift-curve slope increases with increasing lift through the moderate angle-of-attack range at Mach numbers up to about 0.975. This increase in slope is apparently due to a rearward

[illegible] wing [illegible] with increasing angle of attack, which has been observed previously on a thin, unswept wing (ref. 8). At Mach numbers above about 0.975, the main wing shock is probably located at the wing trailing edge at all angles of attack and, therefore, an increasing lift-curve slope with increasing lift no longer exists.

Very high lift coefficients were attained at Mach numbers from 0.95 up. (See fig. 7.) At these Mach numbers lift coefficients of the order of 1.5 were reached at an angle of attack of 22.5° which was the limiting angle of the tests. At lower Mach numbers, stalling begins at much lower angles of attack which would apparently result in considerably lower maximum lift coefficients.

As can be seen in figure 23, the effect of the drooped leading edge on the lift coefficient at $(L/D)_{max}$ was small at Mach numbers up to about 0.94. Also, no appreciable differences in lift characteristics or angle of zero lift exist for the model with and without the 3° droop. (See fig. 6.) An increase in $(L/D)_{max}$ of about 19 percent was realized at a Mach number of 0.80 by utilizing the 3° droop (fig. 23). The improvement diminished as the Mach number was increased. At a Mach number of 0.87, a reasonable cruising speed for an airplane of this type, drooping the leading edge showed an increase in $(L/D)_{max}$ from about 9.0 to 10.2 (13 percent). The values of lift-drag ratio for the model with the drooped leading edge are about 19 percent below the values for the unswept wing and body combination of reference 6 at Mach numbers up to 1.0. It should be pointed out, however, that the values presented in figure 23 were obtained from the complete model which includes the effect of the tail assembly. At Mach numbers above 1.0, the lift-drag ratios are somewhat in error because of wind-tunnel-wall reflected disturbances, but the comparison, which shows about a 7-percent increase as a result of the drooped leading edge, should be valid.

In order to study the behavior of the flow in the boundary layer, instantaneous photographs and motion pictures of the model were obtained during some tests utilizing tufts and the liquid-film flow technique which is described in reference 9. Some of the photographs taken at Mach numbers of 0.80 and 1.00 at moderate and high angles of attack are presented in figure 24. At a Mach number of 0.80, only a small region of separation is evident at 7.7° angle of attack as revealed by the behavior of the tufts. This region is confined to the vicinity of the shock across the wing located at about the 20-percent-chord stations. The presence of the shock is revealed by the discontinuity of the liquid-film flow on the wing. When the angle of attack is increased to 8.8° (approximately the angle at which the lift-curve slope begins to decrease), the flow is separated over nearly the entire wing as can be seen by the erratic nature of the tufts. Movies of the liquid film show that the wing boundary-layer flow at angles of 8.8° and above describes a rotary motion,

moving outboard over the portion of wing behind about the 30-percent root chord station until it reaches approximately the midsemispan, then moving forward toward the leading edge and finally along the forward portion of the wing inward toward the juncture of the leading edge and fuselage. As the angle of attack is increased further, no general change in the boundary layer flow occurs; that is, the flow remains separated over the entire wing.

The liquid film and tufts show that, at a Mach number of 1.00, no large areas of separated flow appear on the wing at any angle of attack up to 22.2°, the maximum angle attained. Some leading-edge separation appears at an angle of attack of about 8°; however, the flow reattaches just behind the separated region. As the angle of attack is increased, the separated area expands chordwise on the wing and appears to extend to about the 10-percent-chord stations at the highest angle.

Effect of tip tanks.- With the wing-tip fuel tanks installed on the model the lift curves become linear at low and moderate angles of attack where an increasing slope with increasing angle was previously noted. (See fig. 11.) Since the tanks are located such that the model cross-sectional area is increased considerably in the region of maximum area (see fig. 3), the main wing shock position remains fixed with increasing angle of attack.

The effect of the tip tanks on the model drag is presented in figure 25. At zero lift, the increment in drag coefficient increases from a value of about 0.0025 at a Mach number of 0.80 to about 0.010 at a Mach number of 1.0. As the lift coefficient is increased to 0.40, the effect of the tanks on the drag is small at Mach numbers up to about 0.96. The increase in effective aspect ratio with the tanks installed reduces the induced drag sufficiently at moderate lift coefficients to compensate for the increased profile and interference drag.

The maximum lift-drag ratio was reduced about 0.9 (8 percent) at a Mach number of 0.80 by addition of the tip tanks. (See fig. 26.) The reduction diminished to a minimum of about 0.15 (2 percent) at a Mach number of about 0.95. A reduction of about 0.4 (approximately 4 percent) was experienced at a Mach number of 0.87.

Dive-flap effectiveness.- The effect of the dive flaps on the model drag coefficient is presented in figure 27. The flaps located at the 52-percent fuselage station mounted 30° up from the plane of symmetry ($WNFVH_0E_1D_2 60$) were considerably more effective in increasing the drag than the flaps on the side of the fuselage just behind the wing ($WNFVH_0E_1D_1 60$). The increase in drag coefficient due to the flaps being open 60° and mounted forward and below the wing was about 0.064 at the lower Mach numbers and about 0.085 at the higher Mach numbers, whereas the increase due to the flaps being open 60° on the sides of the fuselage was about 0.052. It should be pointed out that the effect of the shell

deflectors is not included in the data of figure 27 obtained from tests of the forward dive-flap location $(WNFVH_0E_1D_260)$; however, it can be established from the basic data that they have little influence on any of the model aerodynamic characteristics including the dive-flap effectiveness.

Static Longitudinal Stability

Basic model.- The data presented in figure 18 for the model without the horizontal tail reveal a destabilizing change in the pitching-moment curves at high lift coefficients. It is also evident that this destabilizing characteristic occurs at higher lift coefficients at Mach numbers above 0.90 than at Mach numbers up to 0.90. In the discussion of the liquid-film flow (fig. 24), it was pointed out that a circulatory flow existed on the wing at a Mach number of 0.80 starting at an angle of attack of about 8.8°. The direction of the flow along the wing leading edge was inward toward the juncture of the leading edge and fuselage which suggests that the pressures in this region decreased as the angle was increased to about 8.8°. It is, therefore, possible that the destabilizing break in the pitching-moment curves at the lower Mach number was caused by a forward movement of the center of loading on the inboard portion of the wing. Furthermore, the center of loading on the body in the region adjacent to the wing probably moved forward.

The reasons for the destabilizing tendency noted for the higher Mach numbers at very high angles of attack for the model with no horizontal tail (fig. 18) are not clearly indicated by the flow studies but may be associated with the increasing chordwise extent of flow separation just behind the wing leading edge as the angle of attack is increased.

A comparison of the pitching-moment data given in figures 11 and 12 shows that addition of the horizontal tail increases the severity of the destabilizing tendency at all Mach numbers. The variation of $C_{m_{i_t}}$ and ϵ with angle of attack presented in figures 28 and 29, respectively, reflect the reasons for the aggravated pitching-moment characteristics. The rate of increase in downwash with angle of attack is increasing, while $C_{m_{i_t}}$, which is directly proportional to the effective dynamic pressure at the tail, has begun to decrease at moderately high angles. Although these parameters could not be determined for angles of attack greater than 15°, the trends show that the vertical location of the horizontal tail is unfavorable from the standpoint of maintaining effectiveness at the higher angles of attack.

The drooped wing leading edge had little effect on the static longitudinal stability of the model (see fig. 6); however, it reduced the trim lift coefficient by about 0.05 to 0.15 throughout the Mach number range.

Effect of tip tanks.- Addition of the wing-tip tanks to the model caused a small reduction in the trim lift coefficient (fig. 11). The greatest change was about 0.10 and occurred at Mach numbers from about 0.925 to 0.95. The tanks had a stabilizing effect on the model at low and moderate lift coefficients as can be seen on figures 11, 12, and 31. The more rearward position of the center of loading (fig. 30) indicates that the main wing shock was probably farther back with the tip tanks on. Also, the variation of center-of-loading position with angle of attack is less for the model with the tanks and indicates a smaller chordwise travel of the main wing shock with changing angle.

Effect of auxiliary tail.- In an attempt to eliminate the unstable break in pitching-moment curves at high lift, an auxiliary horizontal tail was mounted at the fuselage reference line with a negative incidence of 2.5°. As shown in figure 18, addition of this tail alone almost completely eliminated the unstable tendencies at high lift which existed for the basic model with no horizontal tail. The low position of the tail places it in a favorable flow field with regard to downwash at high angles of attack. Furthermore, the effective dynamic pressure in the region of the auxiliary tail is probably greater at high angles of attack than exists in the region of the main horizontal tail.

The data presented in figures 7 and 19 show that the auxiliary tail improved the longitudinal characteristics of the complete model (model with the main horizontal tail) at high lift but did not completely eliminate the destabilizing tendency.

Effect of dive flaps.- The data presented in figure 13 show that the dive flaps deflected 60° on the side of the fuselage behind the wing $(WNFVE_1D_160)$ caused a destabilizing effect on the model with the horizontal tail off. With the horizontal tail on, the flaps had a slightly stabilizing effect on the model (fig. 15). Apparently, the flaps reduced the rate of change in downwash with increasing angle of attack in the region of the horizontal tail. Also, as shown in figure 15, deflecting the flaps caused a large increase in the trim lift coefficient. This increase varied from about 0.10 to about 0.35 in lift coefficient through the Mach number range.

The flaps deflected 60° in the location forward and beneath the wing had a stabilizing effect on the model with and without the horizontal tail (figs. 14 and 16). For the tail-on configuration the effect of dive flap deflection on the trim lift coefficient was smaller for this flap location than was measured with the flaps located behind the wing on the side of the fuselage.

Longitudinal Dynamic Stability

Consideration of the dynamic behavior of a full-scale airplane with regard to the unstable break in the pitching-moment curves at the higher angles of attack suggest the possibility of a pitch-up problem. Accordingly, longitudinal dynamic stability calculations were made at a typical Mach number and altitude to determine the response of a full-scale airplane to certain control inputs which might lead to pitch-up. These calculations were made by utilizing the simplified equation of motion derived in reference 10, in which the variation of forward velocity was assumed to be small in order to reduce the general system to two degrees of freedom. Reference 10 shows close agreement between the results from this simplified system with those from the general three-degrees-of-freedom system. The simplified equation used in the time-history calculations is

$$\ddot{\alpha} + \frac{1}{2\tau}\left(C_{L_\alpha} - \frac{C_{m_{\dot{\theta}}} + C_{m_{\dot{\alpha}}}}{2K_y{}^2}\right)\dot{\alpha} - \nu C_m = \nu C_{m_{i_t}} \Delta i_t \tag{1}$$

Since the coefficients of this equation were generally nonlinear, solutions were obtained by the Runge-Kutta method, a method of numerical integration (ref. 11). The data used were for the $WNFVHE_2$ configuration (figs. 9 to 11) and were corrected for the effect of the modified afterbody, adjusted to a center-of-gravity position of $0.15\bar{c}$, and trimmed for steady flight. The present data in the stability system of axes are applicable even though the equations are derived in terms of the wind axes, since the only two aerodynamic coefficients involved, C_L and C_m, are identical in both systems for an unyawed airplane. The following conditions were assumed:

Altitude, ft	40,000
Weight, lb	14,170
I_y about center of gravity, slug-ft^2	40,090
Initial Mach number	0.90
Wing area, sq ft	191

The response of the airplane to a steady rate of tail deflection of -0.5° per second is shown in figure 31. This low value, which represents a gradual pull-up maneuver, was selected to reduce the inertia effects of the airplane with respect to the aerodynamic effects as far as the possible appearance of pitch-up is concerned. Since the limit of the data lies just beyond the unstable break in the static pitching-moment curve, the angle-of-attack response shows only a slight tendency to increase nonlinearly at the highest angles tested. However, the sharp rise of the angular velocity and acceleration curves beginning at about 13.5° angle

of attack indicates that a pitch-up motion has begun, which would be reflected more strongly in the angle-of-attack curve after some time lag. Data at higher angles of attack for another configuration (fig. 7) indicate that the static pitching-moment curve would become more highly unstable if extended to higher angles and thereby aggravating this pitch-up tendency.

The response of the airplane to a steady rate of tail deflection of -2° per second, which represents a practical flight maneuver, is presented in figure 32. This figure also shows the response of the airplane to a corrective control input of 2° per second applied at 12° angle of attack, which is typical of several pull-out maneuvers calculated for various initial angles of attack less than 14°. Good controllability is illustrated by these curves, with the peak angle of attack being reached in each case approximately 0.5 second after the correction was applied. The limits of the data precluded calculation of the complete maneuver when the corrective control was applied at the approximate angle where the static pitching-moment curve becomes neutrally stable (14°). However, extrapolation of the static pitching-moment curves based on the data obtained from tests of the model with ducts faired (fig. 7) indicated that the airplane would no longer be controllable. Although this extrapolation yielded only qualitative results, the computations are felt to represent the behavior of the airplane in view of the fact that the airplane pitching-moment curve would be expected to resemble closely the curve of figure 7.

The short-period stick-fixed oscillations of the airplane in response to a sudden disturbance in trimmed flight have also been computed by using the characteristic part of equation (1) and substituting $C_{m_\alpha}\alpha$ at trim for C_m. The period and time to damp to 1/2 amplitude, presented in figure 33, comply with U. S. Air Force requirements given in reference 12 which specify that the airplane must damp to 1/2 amplitude in 1 cycle.

CONCLUSIONS

The results of an experimental investigation at transonic speeds to determine the longitudinal aerodynamic properties of a fighter-type airplane model with a low-aspect-ratio unswept wing and tee-tail lead to the following conclusions:

1. The transonic rise in drag coefficient at zero lift for the model with zero horizontal-tail incidence is about 0.030.

2. Drooping the forward 15 percent of the wing 3° increases the maximum lift-drag ratio about 13 percent at an assumed cruising Mach number of 0.87. The leading-edge droop reduces the trim lift coefficient

by about 0.05 to 0.15 throughout the Mach number range but has little effect on the model stability.

3. At high angles of attack, the model becomes longitudinally unstable at Mach numbers from 0.80 to 0.90. At higher Mach numbers, the model experiences a reduction in static stability when very high angles of attack are reached.

4. Addition of the auxiliary horizontal tail reduces the severity of the unstable break in the static pitching-moment curves which occurs at high angles of attack.

5. Addition of the wing-tip fuel tanks reduces the maximum lift-drag ratio by about 0.9 (8 percent) at a Mach number of 0.80. This reduction diminishes to about 0.15 (2 percent) at a Mach number of 0.95. The tanks cause a small change in the trim lift coefficient and have a stabilizing effect on the model at low and moderate lift coefficients.

6. The dive flaps located ahead of and beneath the wing are 35 percent to 65 percent more effective in increasing the drag than the flaps on the side of the fuselage directly behind the wing. The forward location of the flaps causes a smaller change in the trim lift coefficient than the location behind the wing.

7. Calculations of the dynamic behavior of a full-scale airplane indicate that a pitch-up should be expected, following closely the unstable break in the static pitching-moment curve. Controllability in pitch is good at angles of attack below this break, but a typical corrective control applied after the point of neutral stability has been reached has little effect in averting pitch-up. The period and damping of the short-period stick-fixed oscillations were found to meet U. S. Air Force requirements which state that the airplane must damp to 1/2 amplitude in 1 cycle.

Langley Aeronautical Laboratory,
National Advisory Committee for Aeronautics,
Langley Field, Va., November 8, 1954.

REFERENCES

1. Smith, Willard G.: Wind-Tunnel Investigation at Subsonic and Supersonic Speeds of a Fighter Model Employing a Low-Aspect-Ratio Unswept Wing and a Horizontal Tail Mounted Well Above the Wing Plane - Longitudinal Stability and Control. NACA RM A54D05, 1954.

2. Sleeman, William C., Jr., and Wiggins, James W.: Experimental Investigation at High Subsonic Speeds of the Rolling Stability Derivatives of a Complete Model With an Aspect-Ratio-2.53 Wing Having an Unswept 72-Percent-Chord Line and a High Horizontal Tail. NACA RM L54I20, 1954.

3. Arabian, Donald D., and Schmeer, James W.: Lateral Stability and Control Measurements of a Fighter-Type Airplane Model With a Low-Aspect-Ratio Wing and a Tee-Tail. NACA RM L55F08, 1956.

4. Ward, Vernon G., Whitcomb, Charles F., and Pearson, Merwin D.: Air-Flow and Power Characteristics of the Langley 16-Foot Transonic Tunnel With Slotted Test Section. NACA RM L52E01, 1952.

5. Hallissy, Joseph M., and Bowman, Donald R.: Transonic Characteristics of a 45° Sweptback Wing-Fuselage Combination. Effect of Longitudinal Wing Position and Division of Wing and Fuselage Forces and Moments. NACA RM L52K04, 1953.

6. Kelly, Thomas C.: Transonic Wind-Tunnel Investigation of the Effects of Body Indentation for Boattail and Cylindrical Afterbody Shapes on the Aerodynamic Characteristics of an Unswept-Wing—Body Combination. NACA RM L54A08, 1954.

7. Jones, Robert T.: Theory of Wing-Body Drag at Supersonic Speeds. NACA RM A53H18a, 1953.

8. Hieser, Gerald, Henderson, James H., and Swihart, John M.: Transonic Aerodynamic and Loads Characteristics of a 4-Percent-Thick Unswept-Wing—Fuselage Combination. NACA RM L54B24, 1954.

9. West, F. E., Jr., and Henderson, James H.: Relationship of Flow Over a 45° Sweptback Wing With and Without Leading-Edge Chord-Extensions to Longitudinal Stability Characteristics at Mach Numbers From 0.60 to 1.03. NACA RM L53H18b, 1953.

10. Campbell, George S., and Weil, Joseph: The Interpretation of Nonlinear Pitching Moments in Relation to the Pitch-Up Problem. NACA RM L53I02, 1953.

The Johns Hopkins Press (Baltimore), 1950.

12. Anon.: Military Specification - Flying Qualities of Piloted Airplanes. MIL-F-8785(ASG), Sept. 1, 1954. (Amendment-1, Oct. 19, 1954.)

TABLE I

TEST CONDITIONS

Configuration	Figure	Mach number range	Angle-of-attack range, deg
WNF	5	0.80 to 1.06	0 to 15.9
$WFVH_0$	6	.80 to 1.06	-2.3 to 16.0
$WNFVH_0$	6	.80 to 1.09	-2.3 to 15.9
$WNFVH_{+4}$	7	.80 to 1.06	0 to 22.5
$WNFVH_0E$	8	.80 to 1.09	-2.3 to 15.9
$WNFVH_{+4}E_2$	9	.80 to 1.06	-2.3 to 16.0
$WNFVH_{-8}E_2$	10	.80 to 1.06	-2.2 to 16.0
$WNFVH_0E_2$	11	.80 to 1.09	-2.3 to 15.9
$WNFVH_0E_2T$	11	.80 to 1.00	-2.3 to 16.0
$WNFVE_2$	12	.80 to 1.06	-2.3 to 16.0
$WNFVE_2T$	12	.80 to 1.06	-2.4 to 16.1
$WNFVE_1$	13 and 14	.80 to 1.06	-2.3 to 15.9
$WNFVE_1D_160$	13	.80 to 1.06	-2.3 to 11.3
$WNFVE_1D_360$	14	.80 to 1.06	-2.5 to 11.2
$WNFVH_0E_1$	15 and 16	.80 to 1.06	-2.3 to 15.9
$WNFVH_0E_1D_160$	15	.80 to 1.06	-2.3 to 11.3
$WNFVH_0E_1D_260$	16	.80 to 1.06	-2.4 to 11.2
$WNFVH_0E_1D_130$	17	.80 to 1.06	-2.3 to 11.4
WNFV	18	.80 to 1.06	0 to 22.5
$WNFVH_A$	18	.80 to 1.06	0 to 22.5
$WNFVH_{+4}H_A$	19	.80 to 1.06	0 to 22.5

	Wing	Horizontal tail
Aspect ratio	2.5	2.97
Taper ratio	.385	.311
Area	202.5 in.^{2}	51.25 in.^{2}
Span	22.50	12.328
Root chord	13.00	6.341
Tip chord	5.00	1.974
Section	Modified biconvex	Modified biconvex
Thickness ratio		
Root	3.4 percent	5 percent
Tip	3.4 percent	3 percent

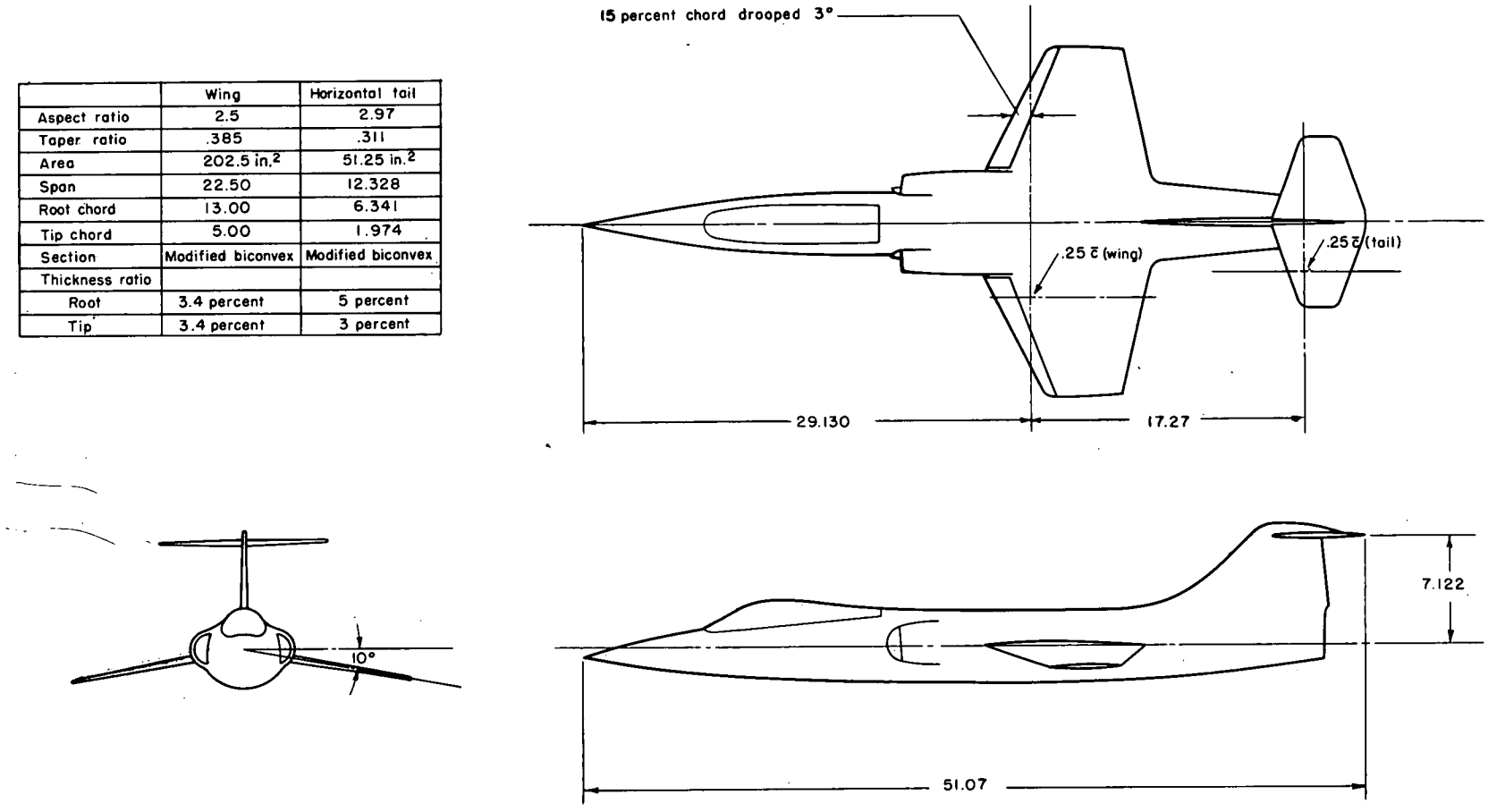

(a) Principal dimensions.

Figure 1.- Sketches of the model. All dimensions are in inches.

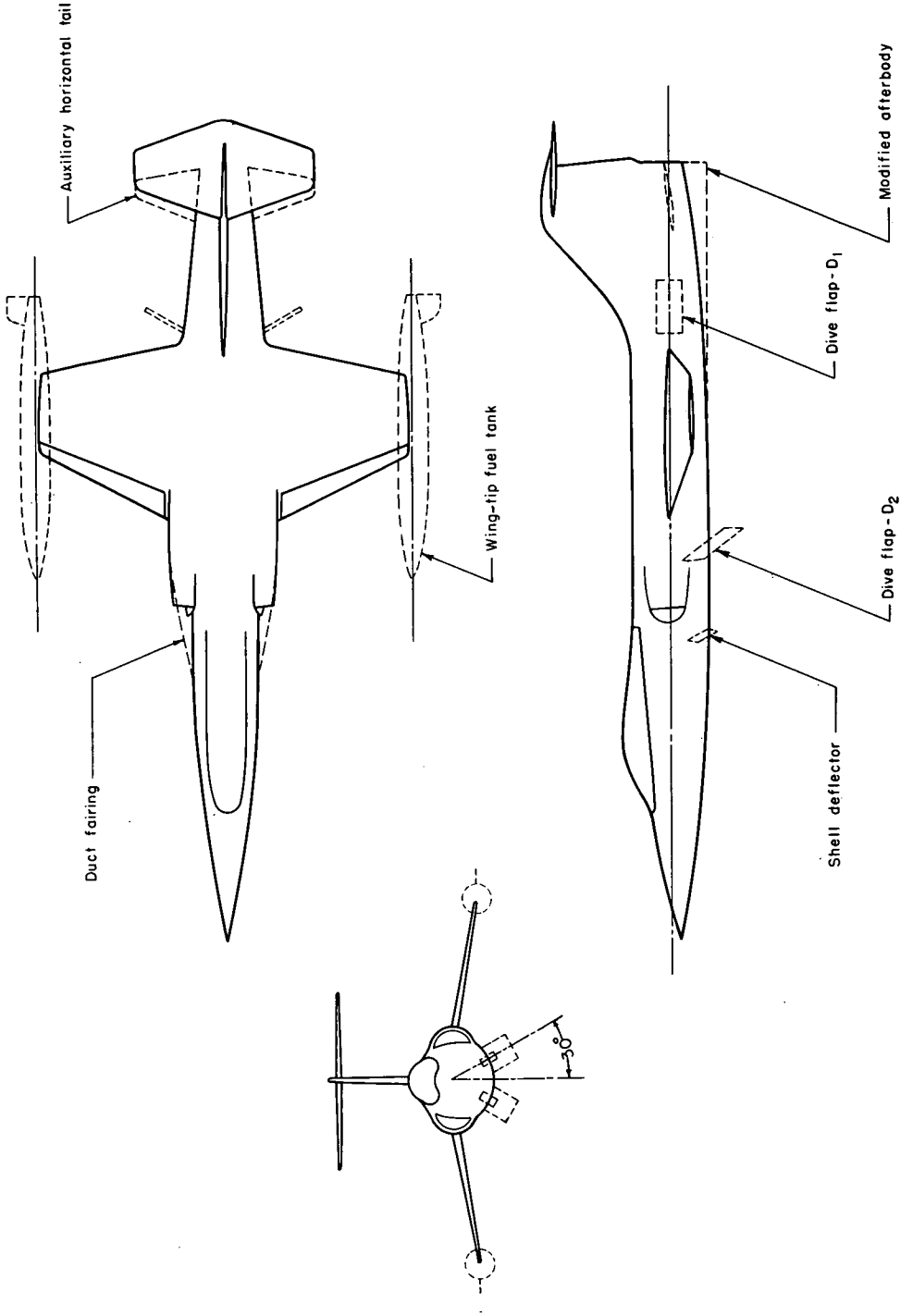

(b) Alternate configurations.

Figure 1.- Concluded.

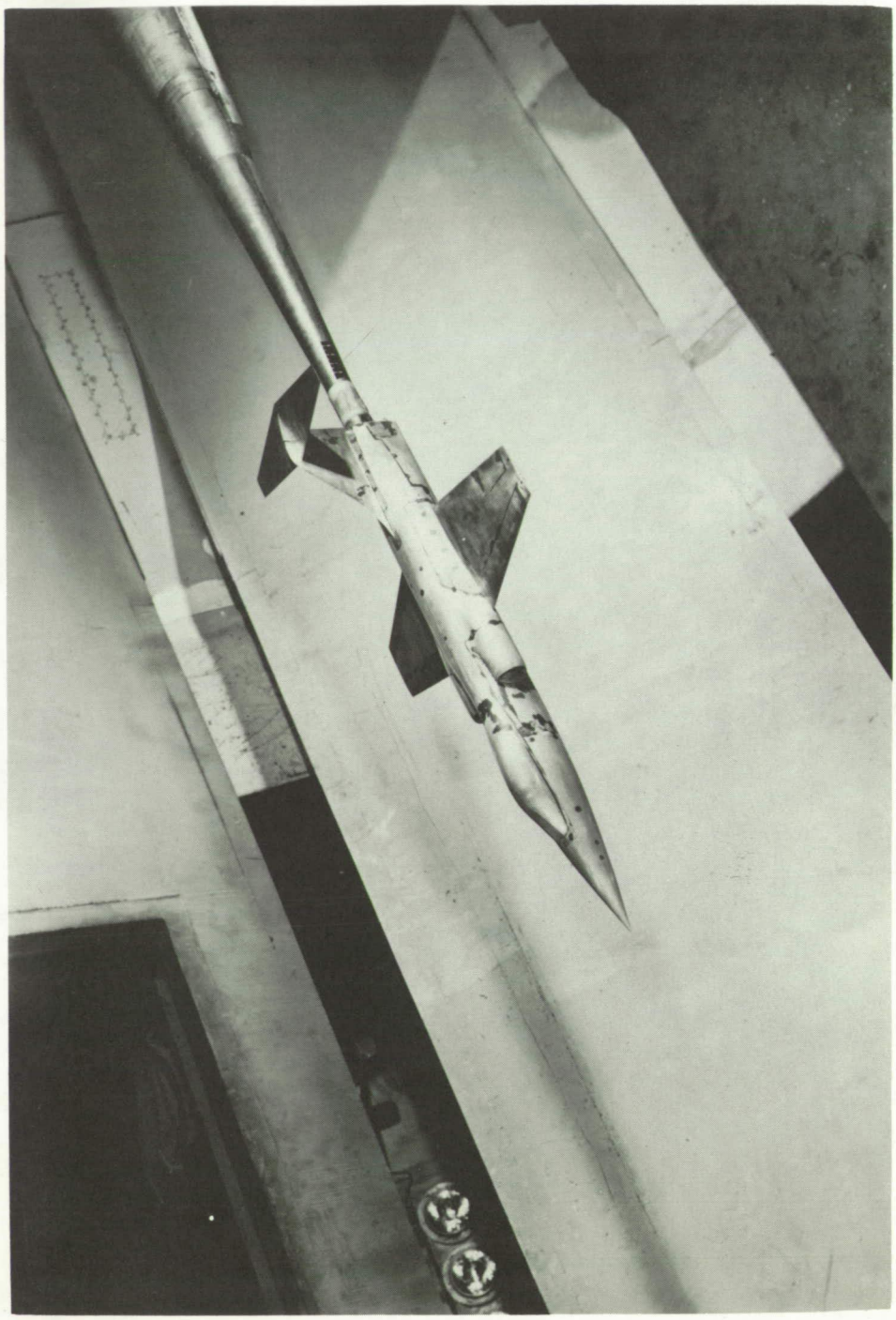

L-81864

(a) $WNFVH_OE_2$ configuration.

Figure 2.- Photographs of the model mounted in the Langley 16-foot

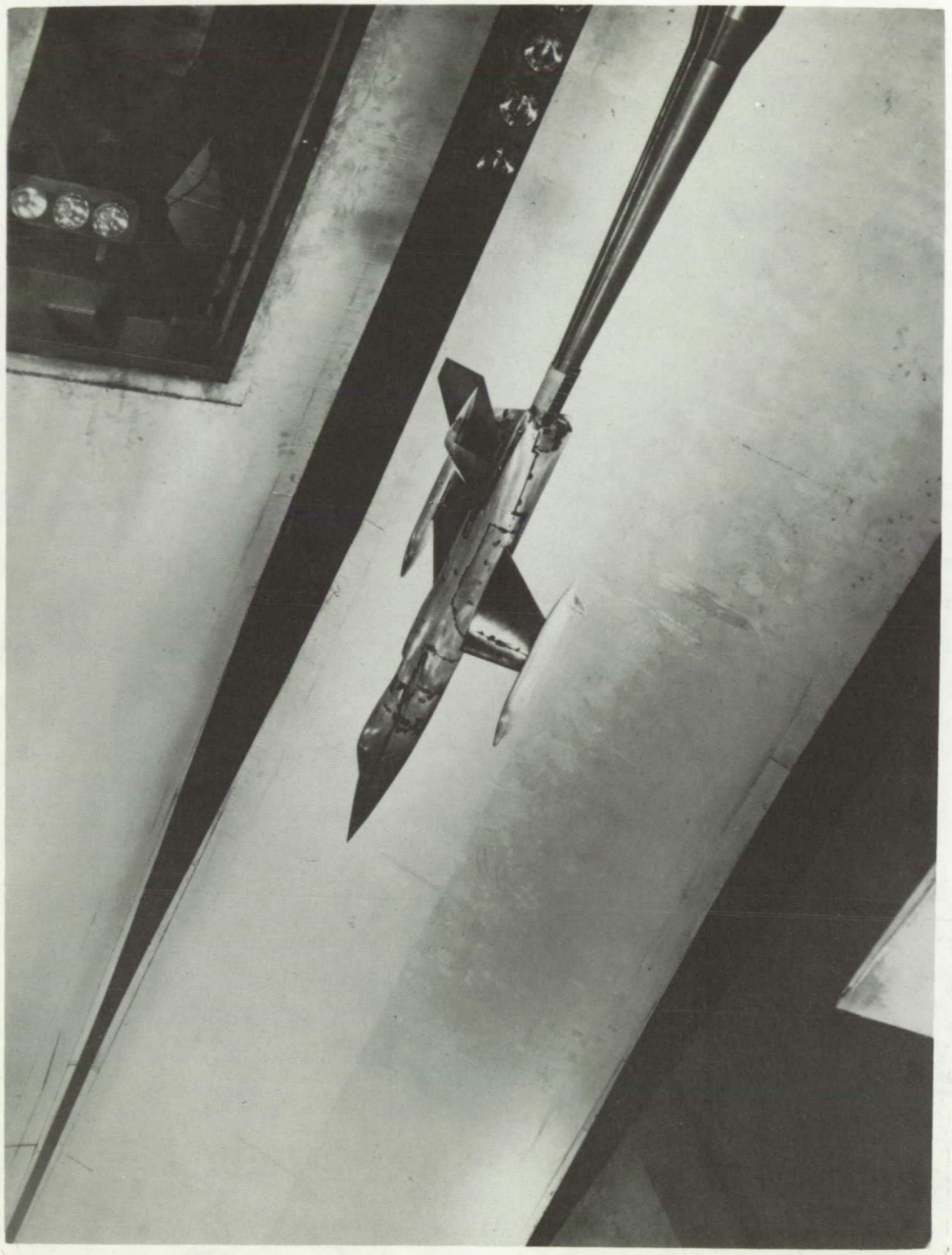

L-81829

(b) $WNFVH_0E_2T$ configuration.

Figure 2.- Continued.

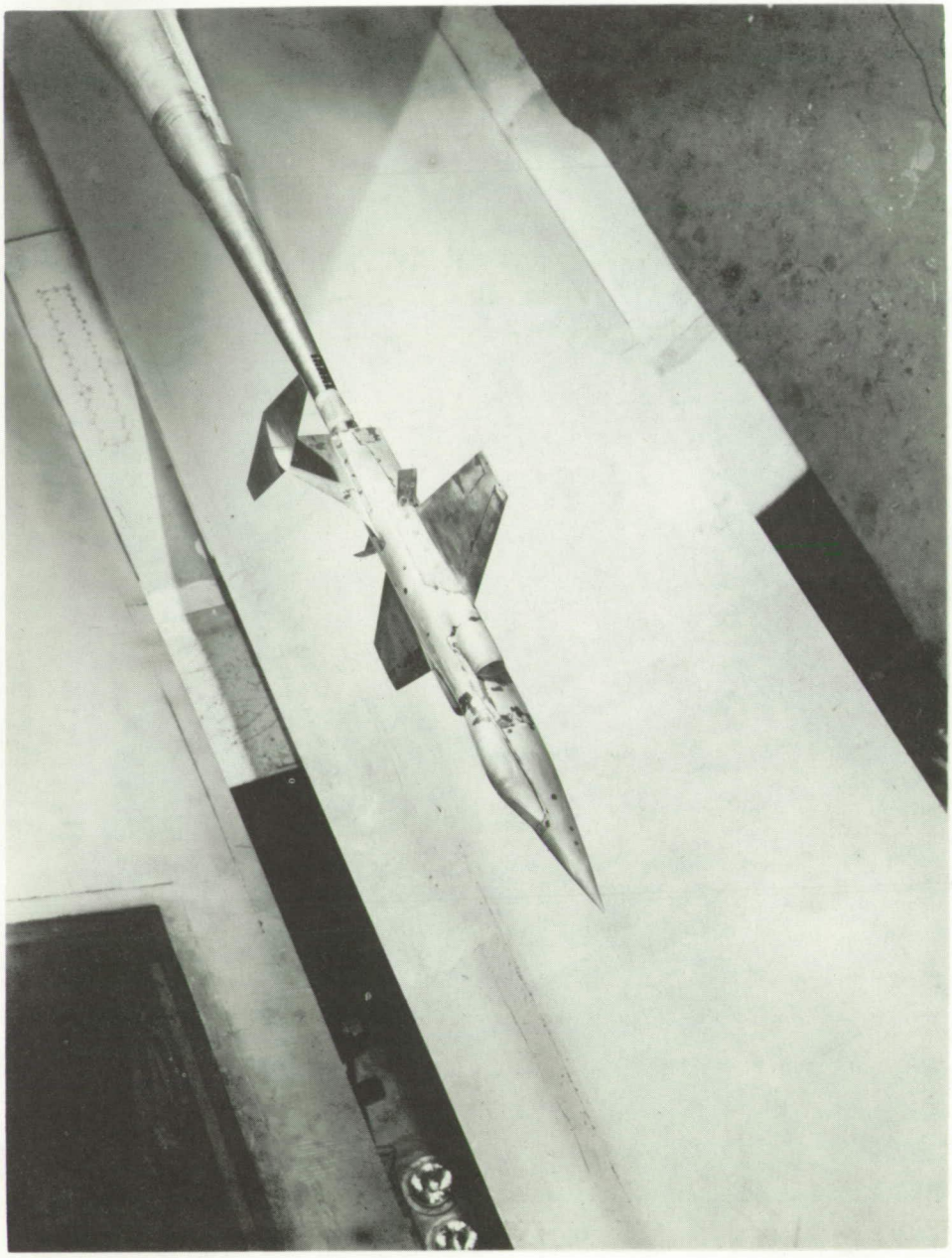

L-81871

(c) $WNFVH_{0_1}E_1D_1$60 configuration.

Figure 2.- Continued.

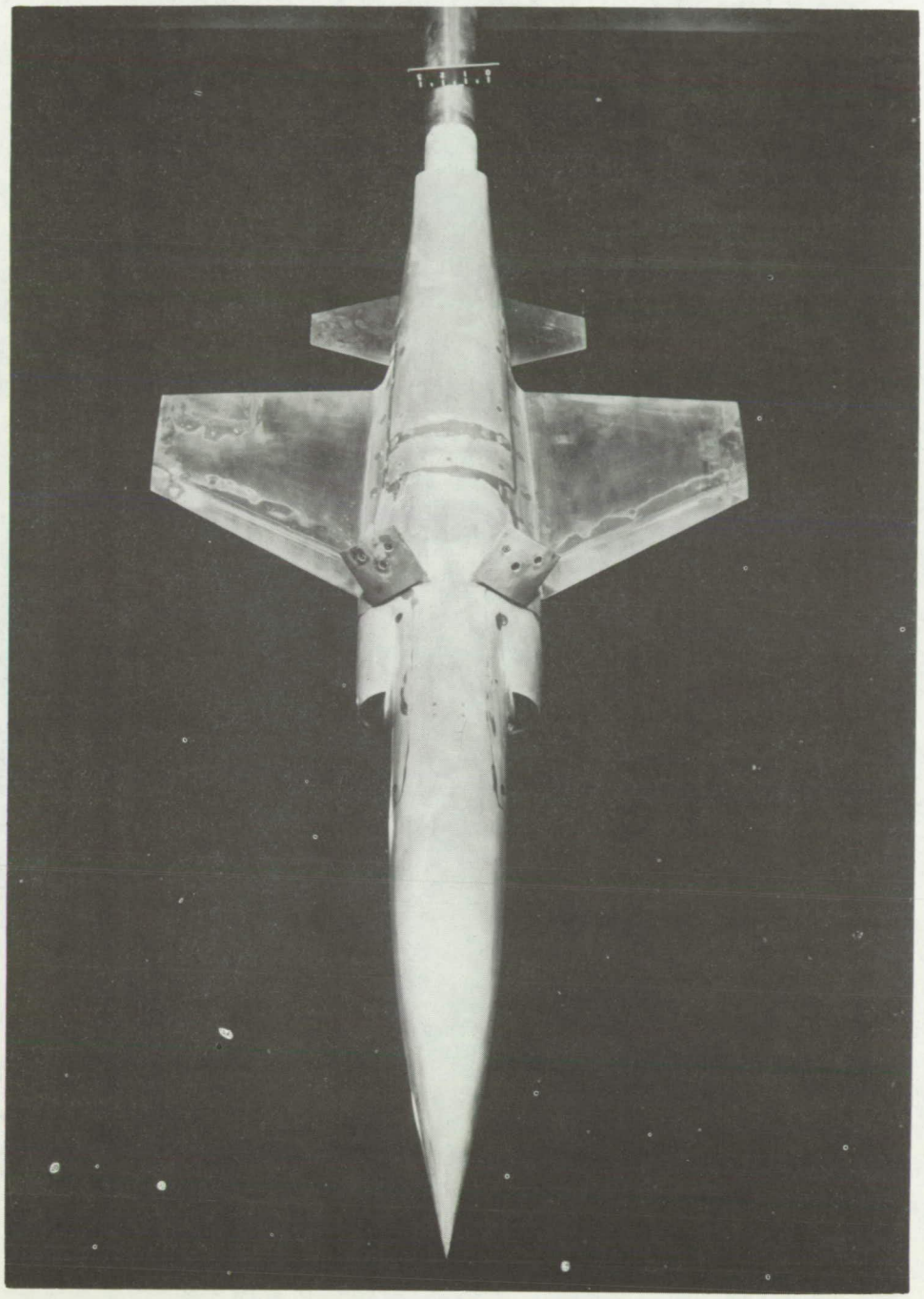

L-81868

(d) $WNFVH_0E_1D_2$60 configuration.

Figure 2.- Continued.

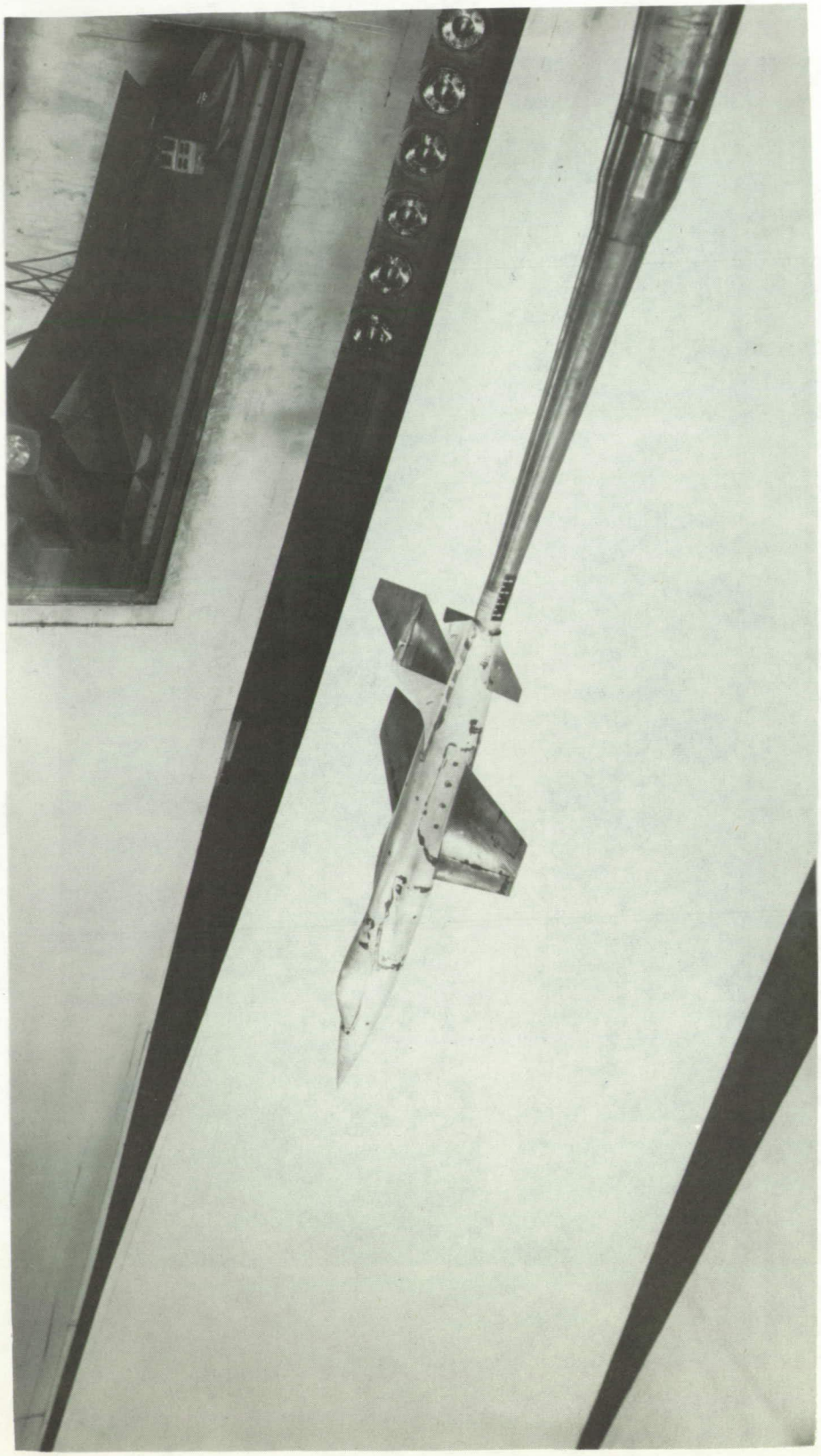

L-81955

(e) $WNFVH_{+4}H_A$ configuration.

Figure 2.- Concluded.

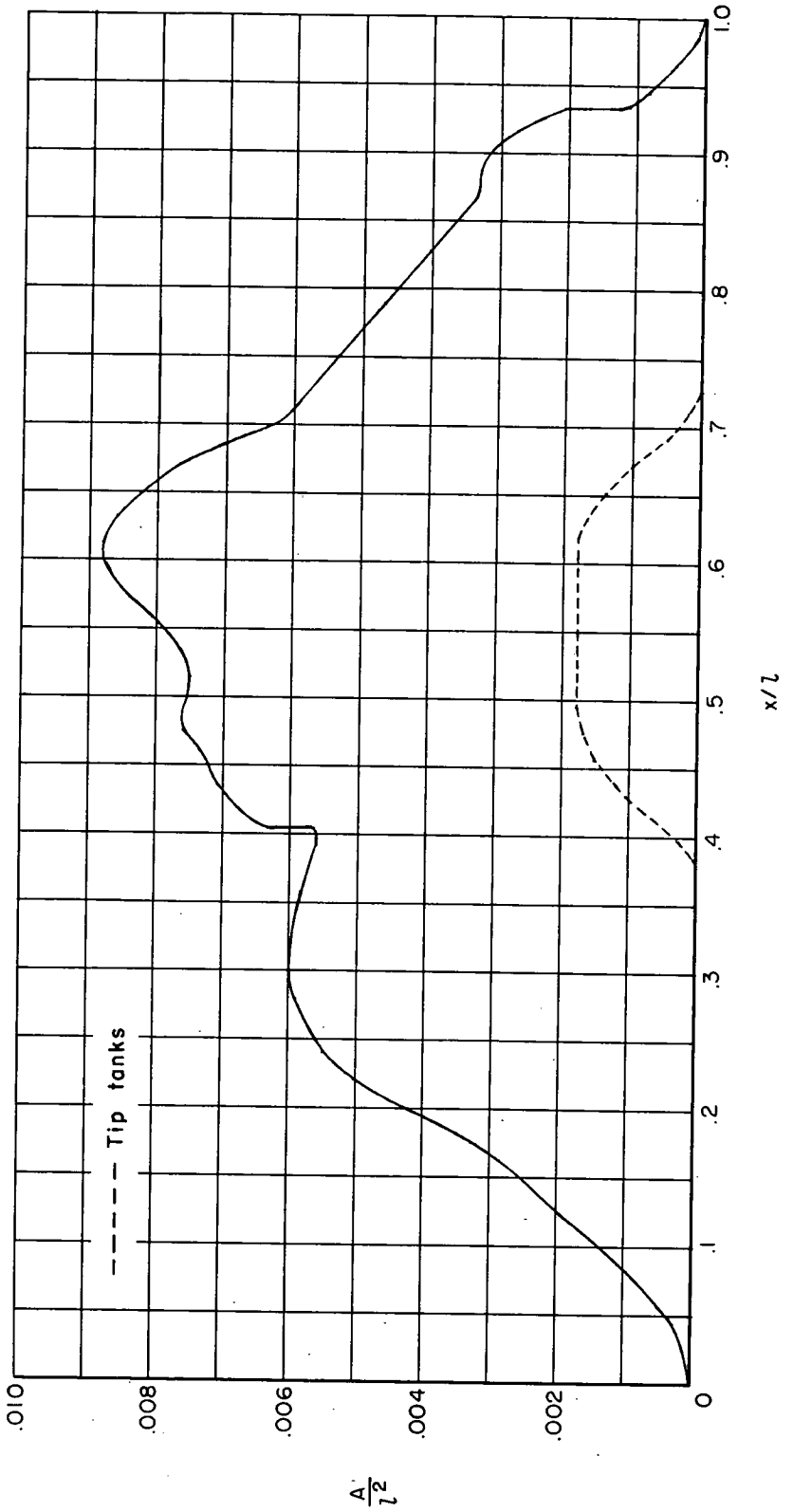

Figure 3.- Longitudinal distribution of cross-sectional area. Model with ducts opened and 80 percent of duct inlet area removed from duct entrance to end of tail pipe; afterbody not modified.

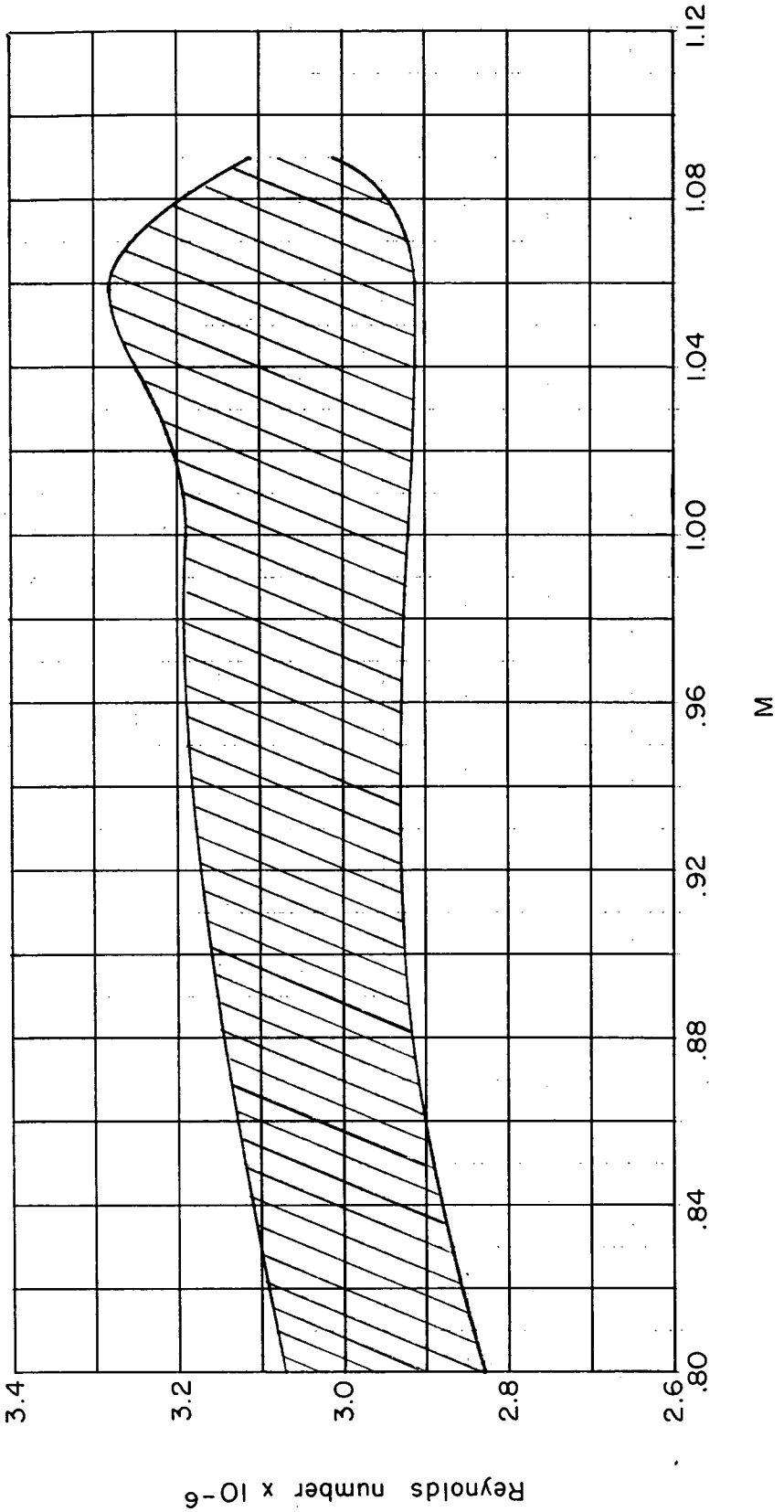

Figure 4.- Variation of Reynolds number based on wing mean aerodynamic chord over the Mach number range covered by the tests.

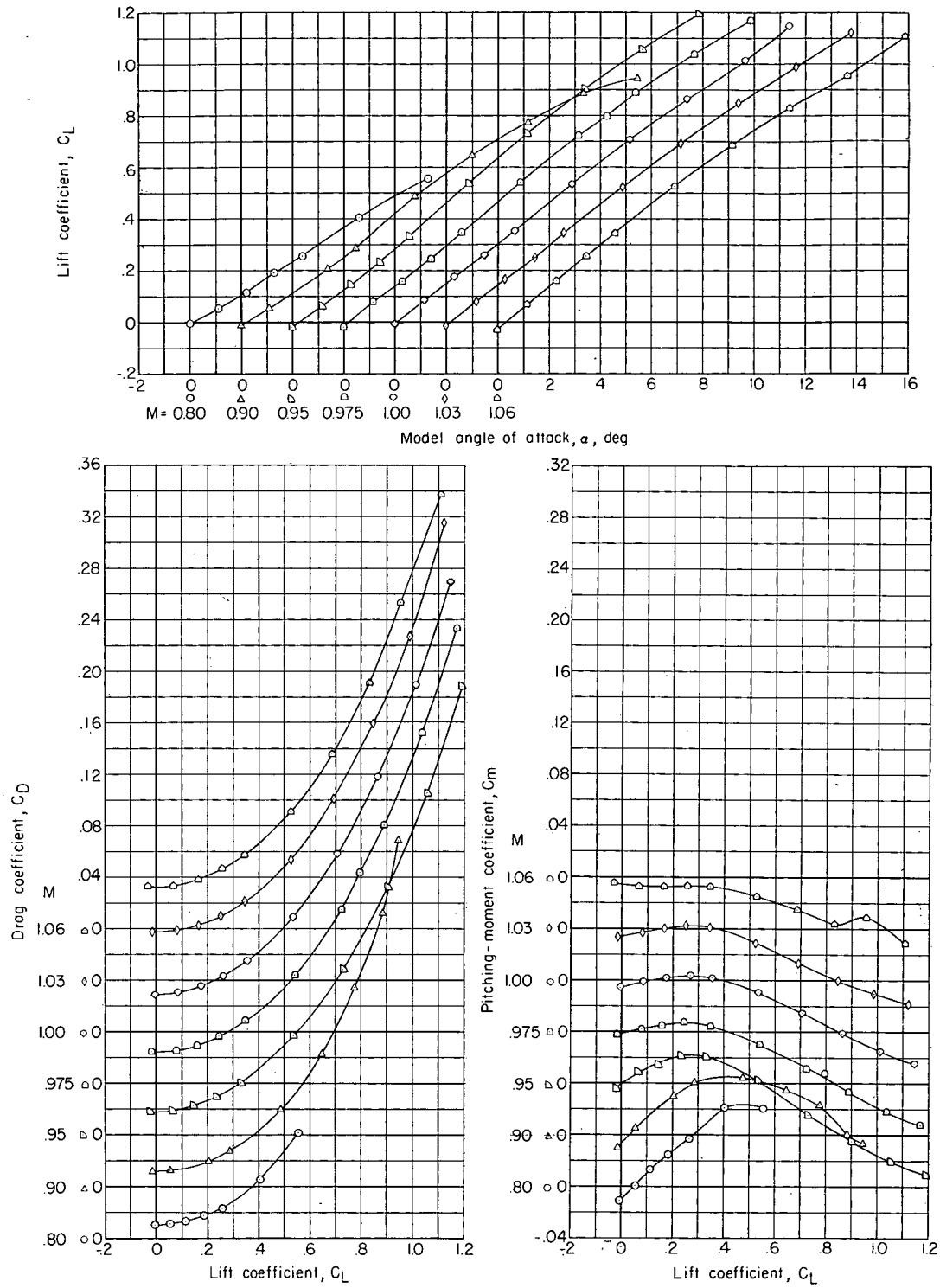

Figure 5.- Lift, drag, and pitching-moment characteristics. WNF configuration.

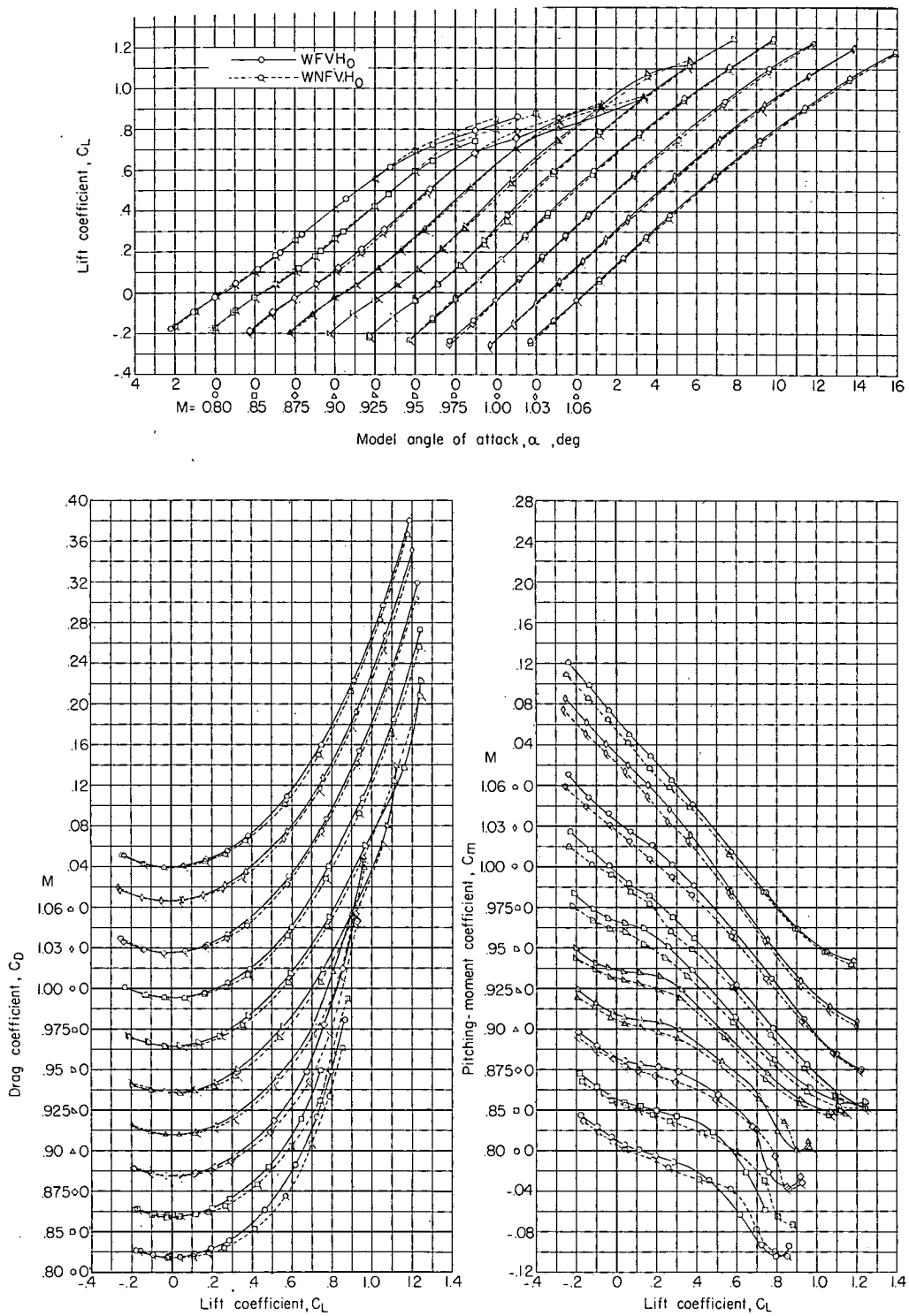

Figure 6.- Lift, drag, and pitching-moment characteristics. $WNFVH_0$ and $WFVH_0$ configurations.

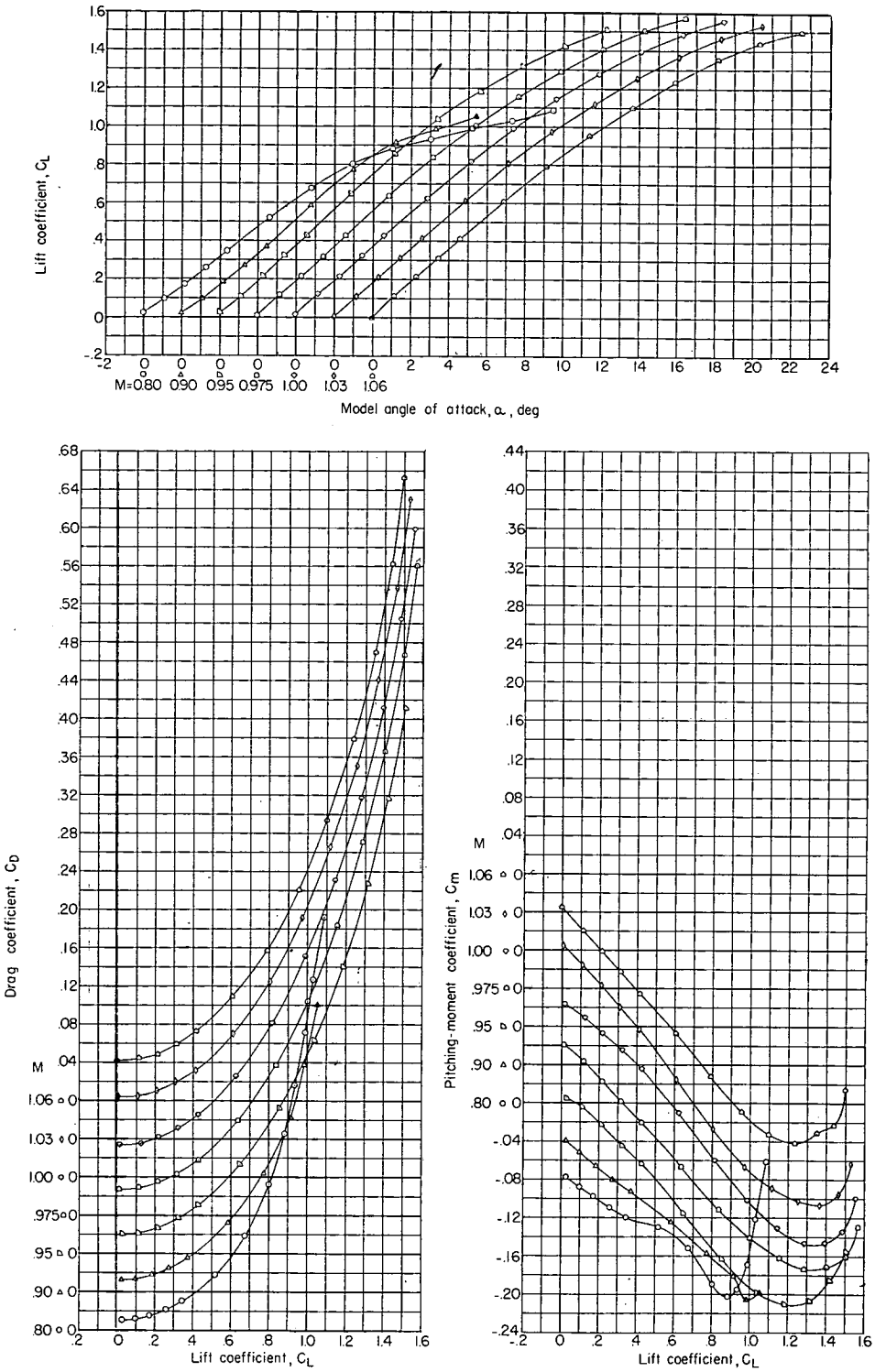

Figure 7.- Lift, drag, and pitching-moment characteristics. $WNFVH_{+4}$ configuration.

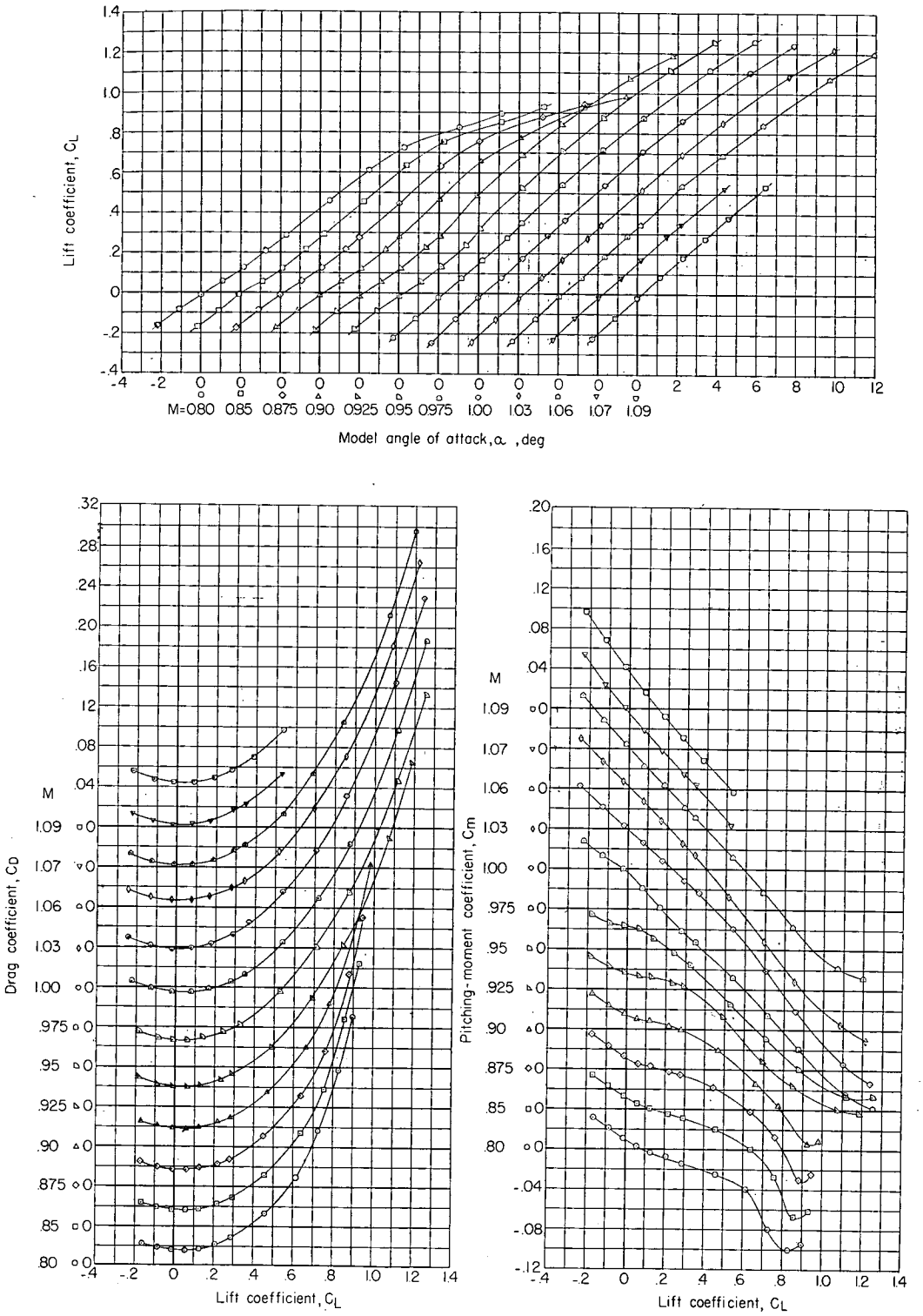

Figure 8.- Lift, drag, and pitching-moment characteristics. $WNFVH_0E$ configuration.

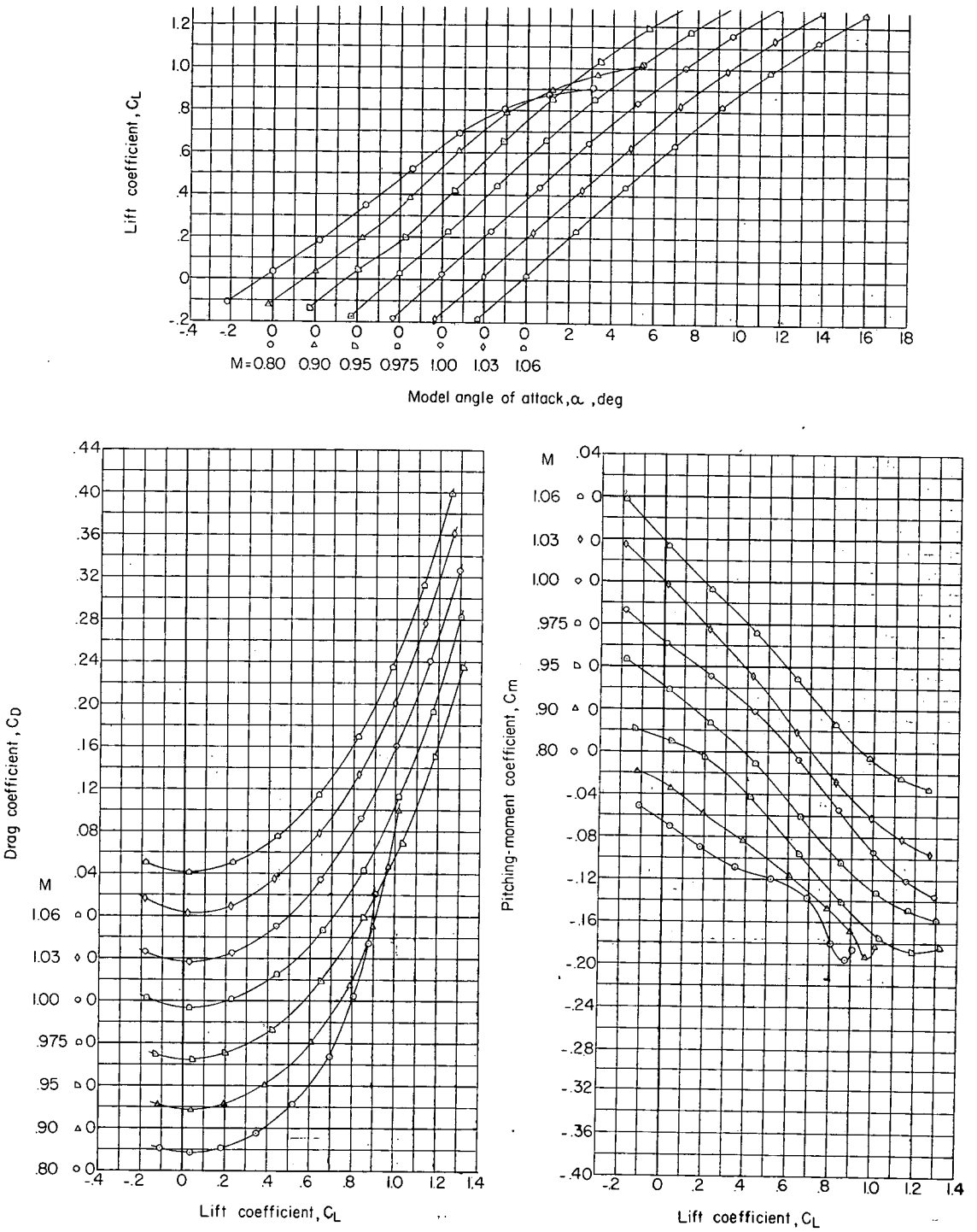

Figure 9.- Lift, drag, and pitching-moment characteristics. $WNFVH_{+4}E_2$ configuration.

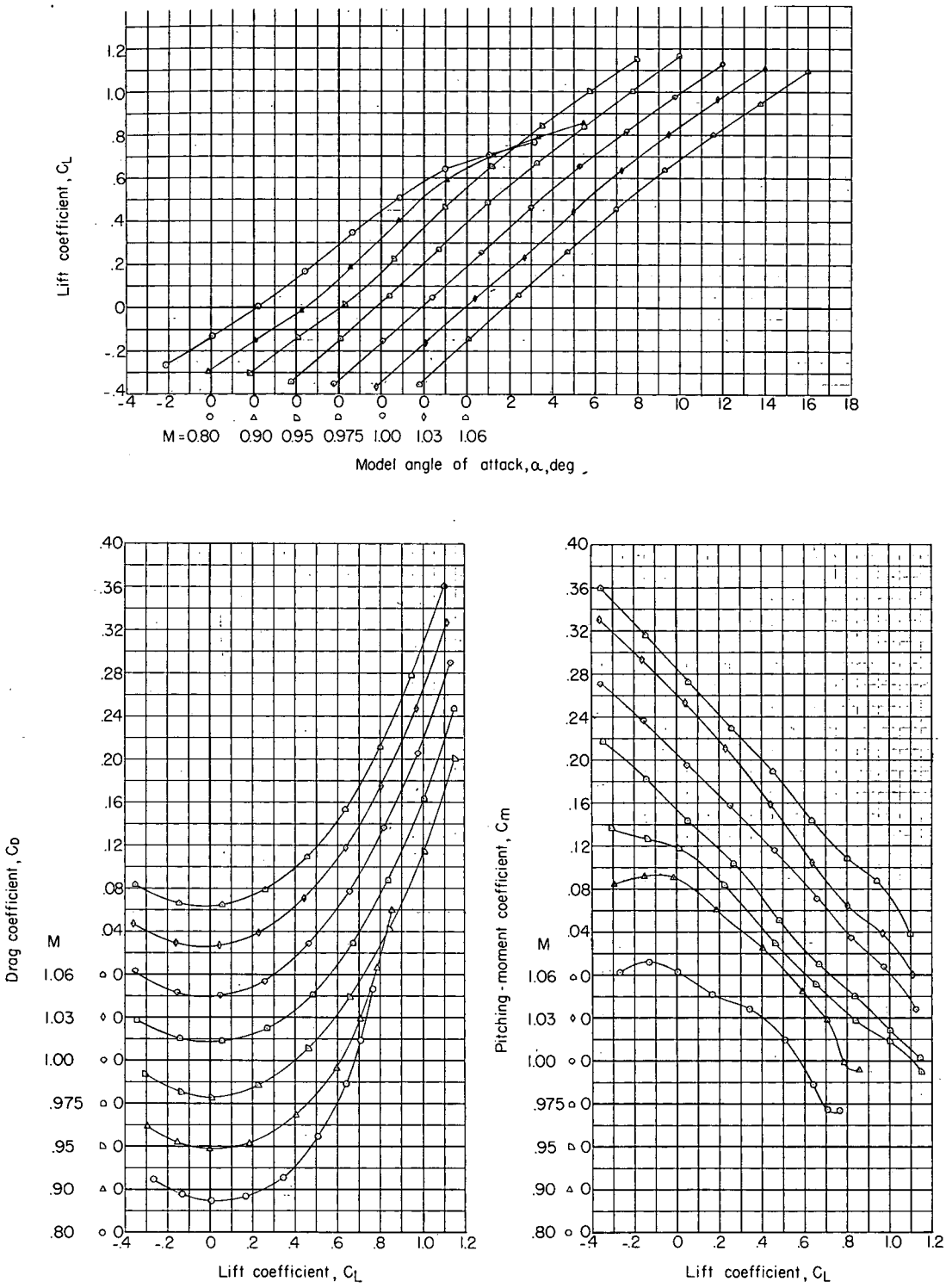

Figure 10.- Lift, drag, and pitching-moment characteristics. $WNFVH_{-8}E_2$ configuration.

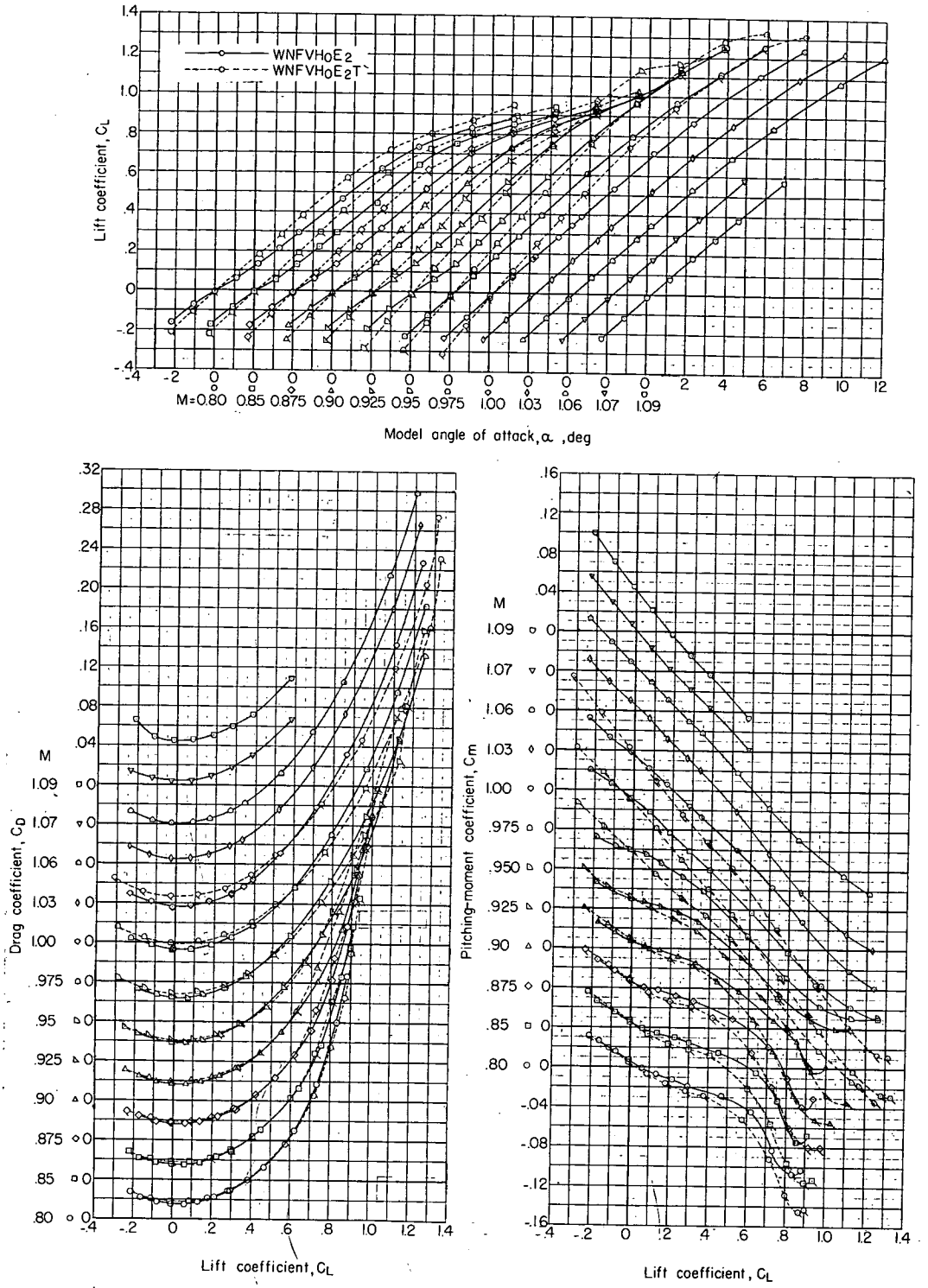

Figure 11.- Lift, drag, and pitching-moment characteristics. $WNFVH_0E_2$ and $WNFVH_0E_2T$ configurations.

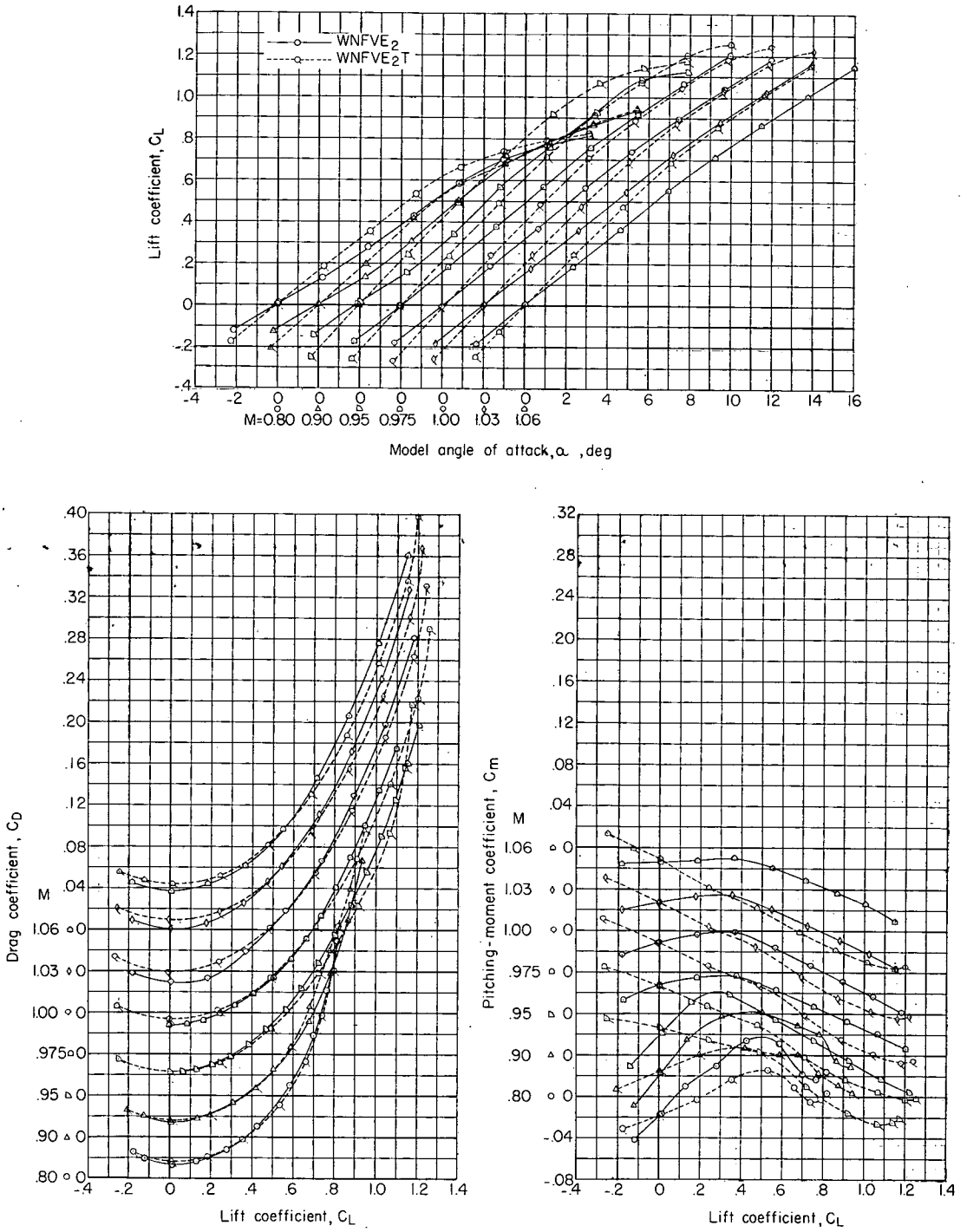

Figure 12.- Lift, drag, and pitching-moment characteristics. WNFVF and $WNFVE_2T$ configurations.

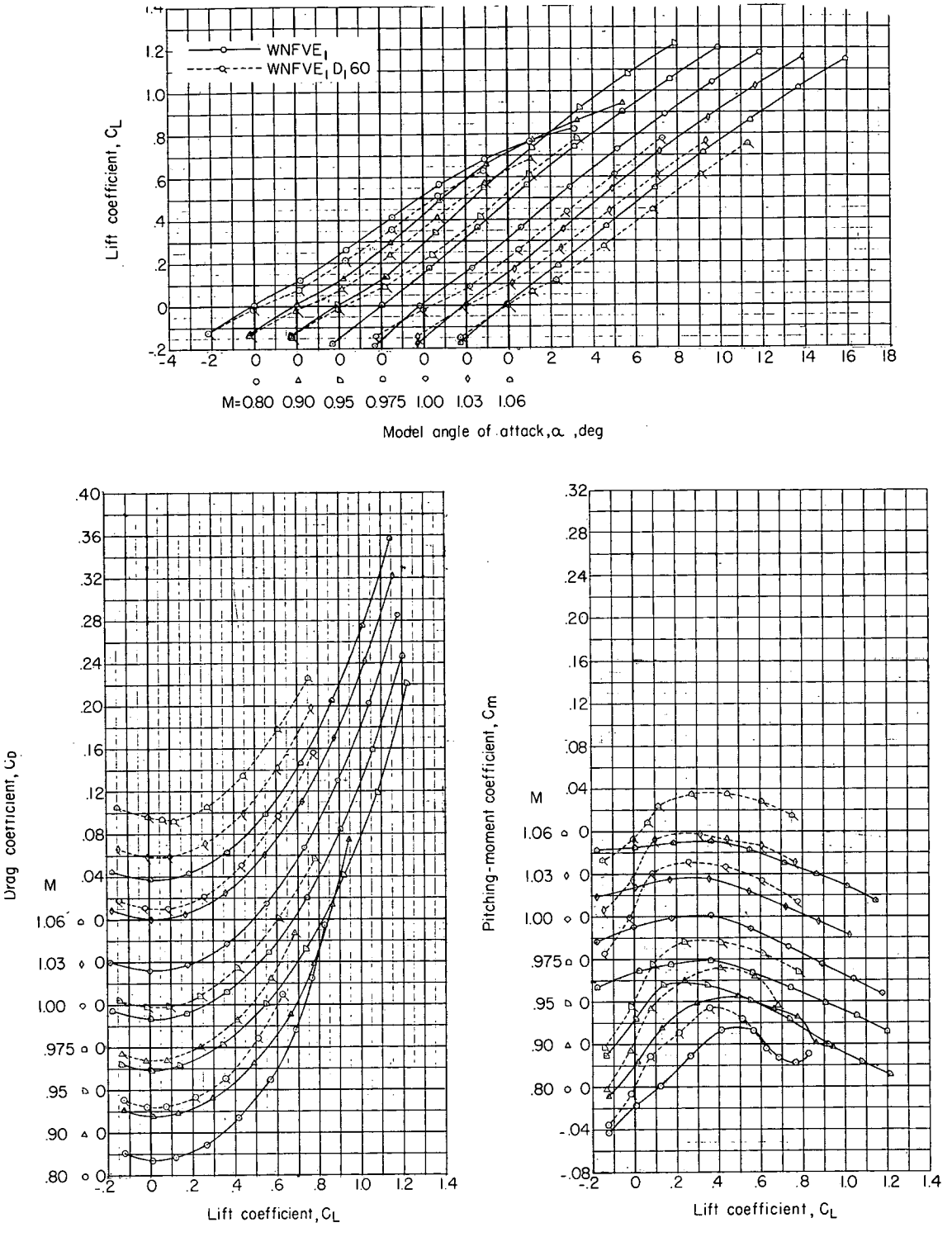

Figure 13.- Lift, drag, and pitching-moment characteristics. WNFVE- and WNFVE-D 60 configurations.

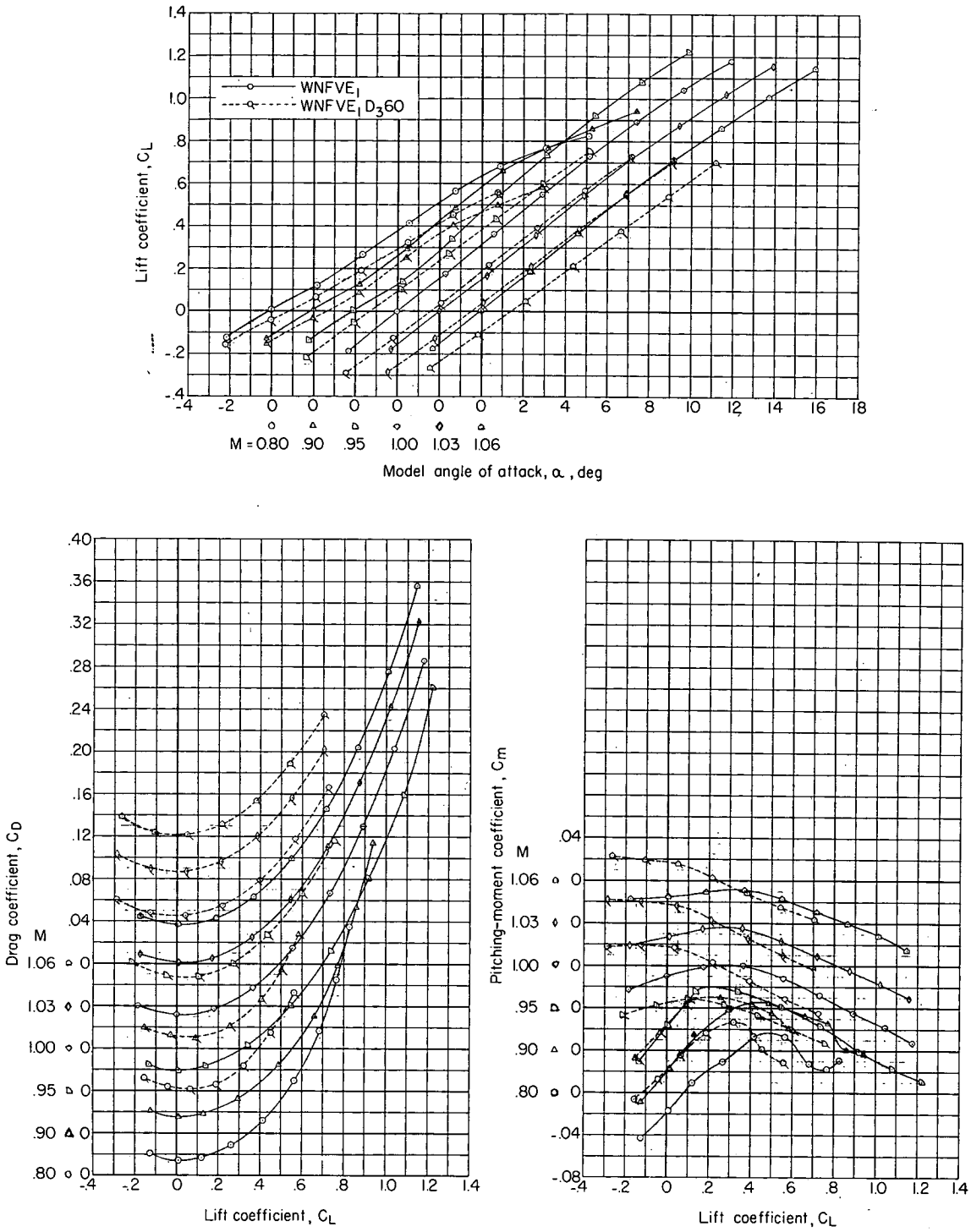

Figure 14.- Lift, drag, and pitching-moment characteristics. $WNFVE_1$ and $WNFVE_1D_360$ configurations.

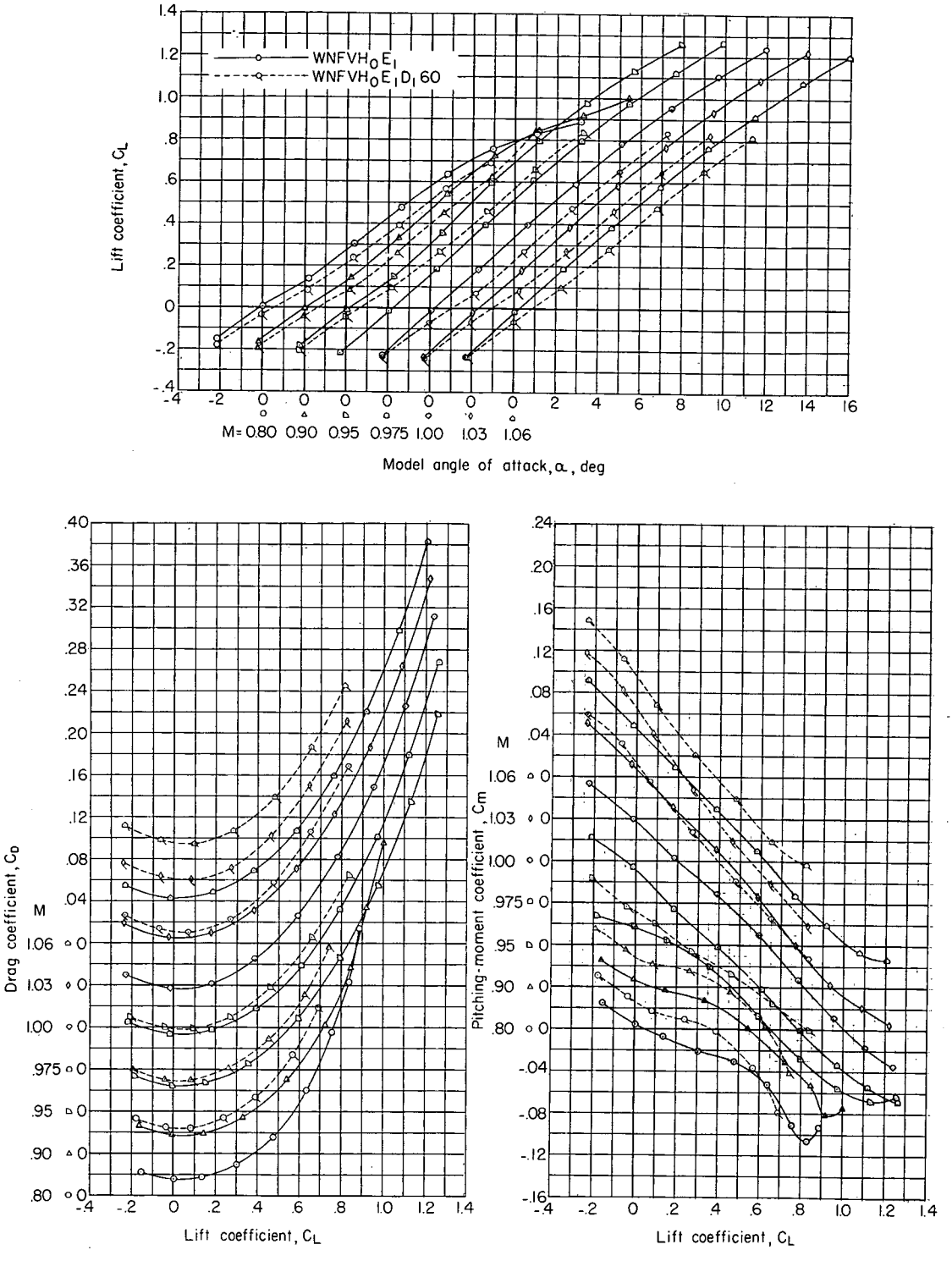

Figure 15.- Lift, drag, and pitching-moment characteristics. WNFVH$_0$E$_1$ and WNFVH$_0$E$_1$D$_1$60 configurations.

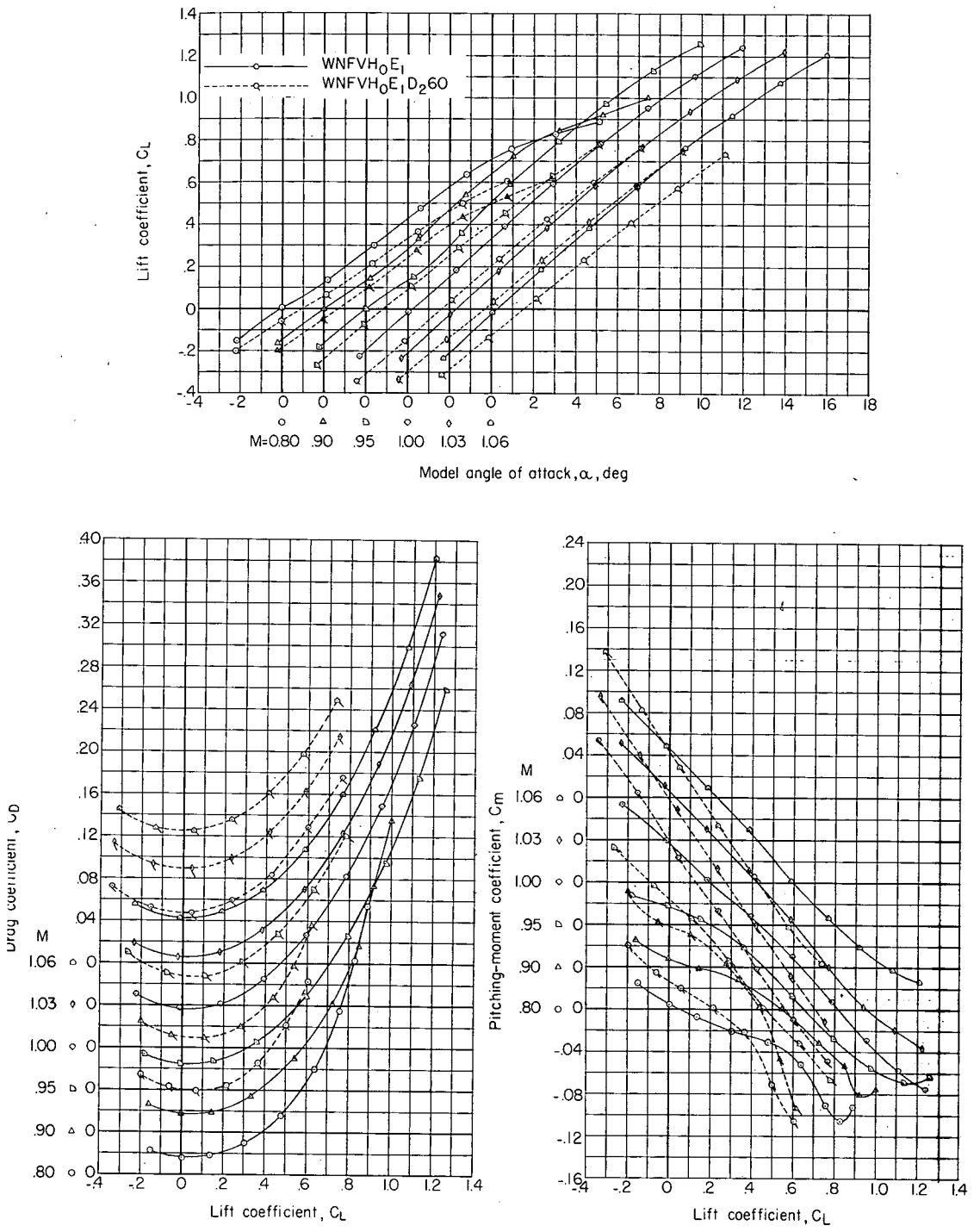

Figure 16.- Lift, drag, and pitching-moment characteristics. WNFVH$_0$E$_1$ and WNFVH$_0$E$_1$D$_2$60 configurations.

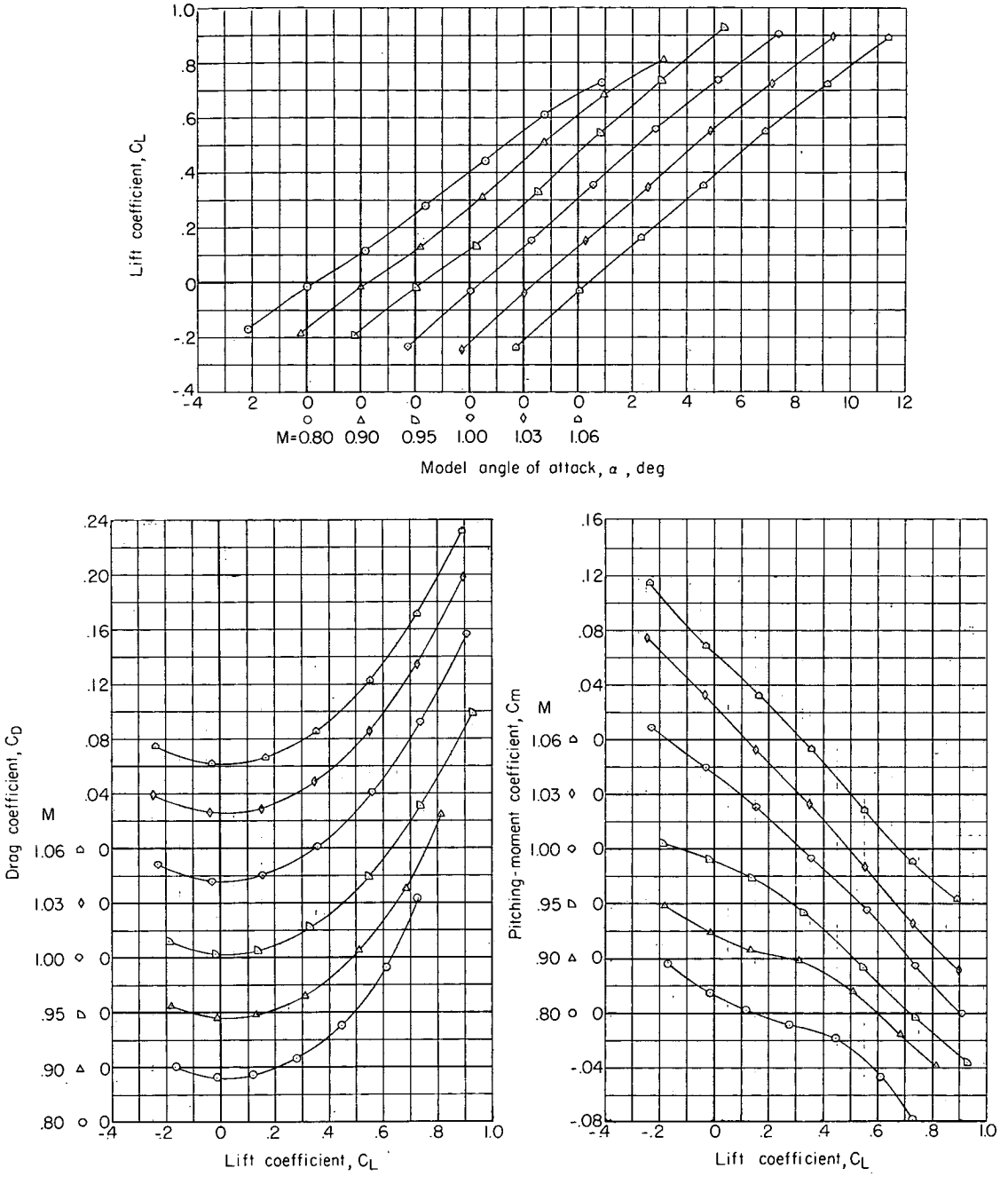

Figure 17.- Lift, drag, and pitching-moment characteristics. $WNFVH_0E_1D_1 30$ configuration.

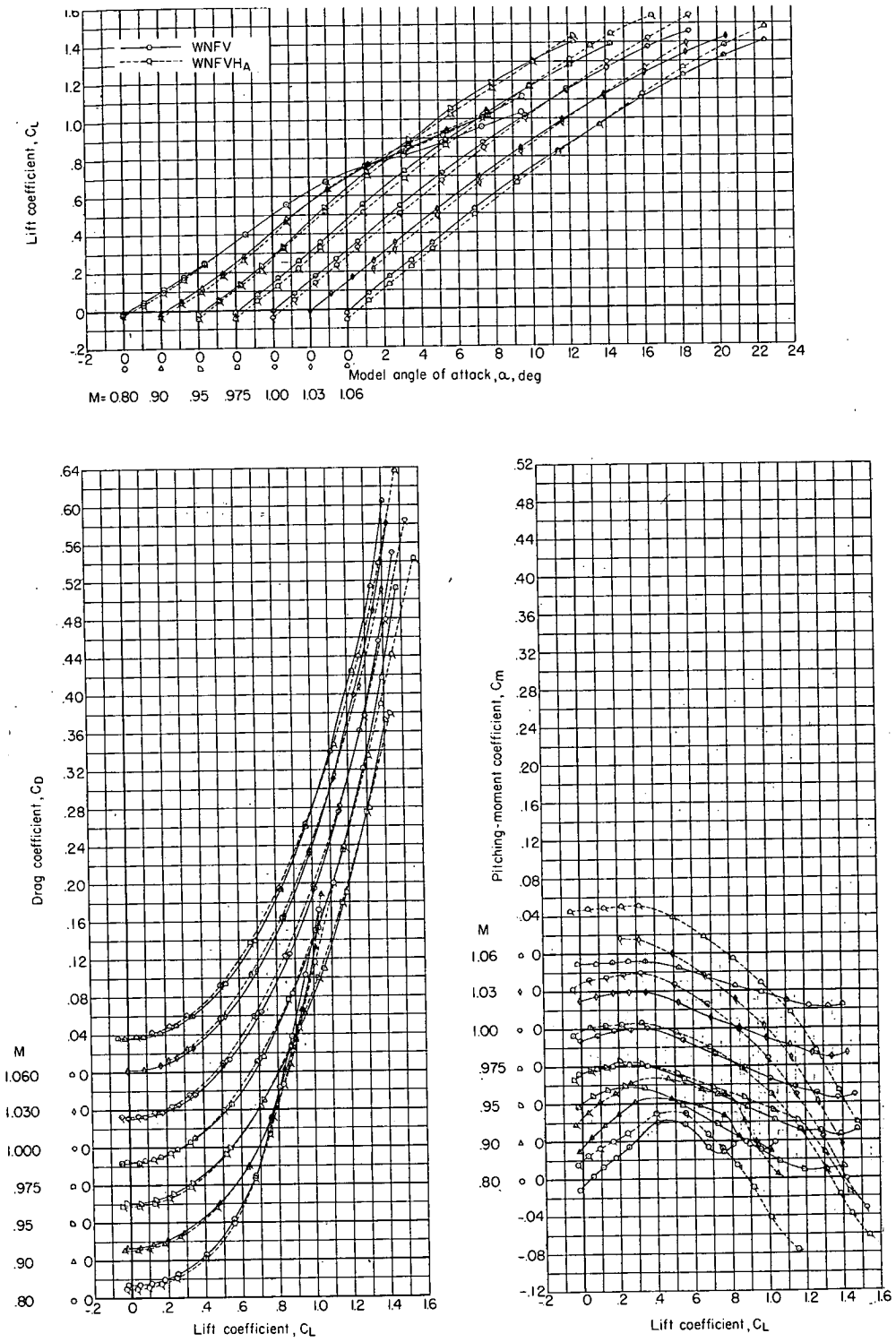

Figure 18.- Lift, drag, and pitching-moment characteristics. WNFV and WNFVH$_A$ configurations.

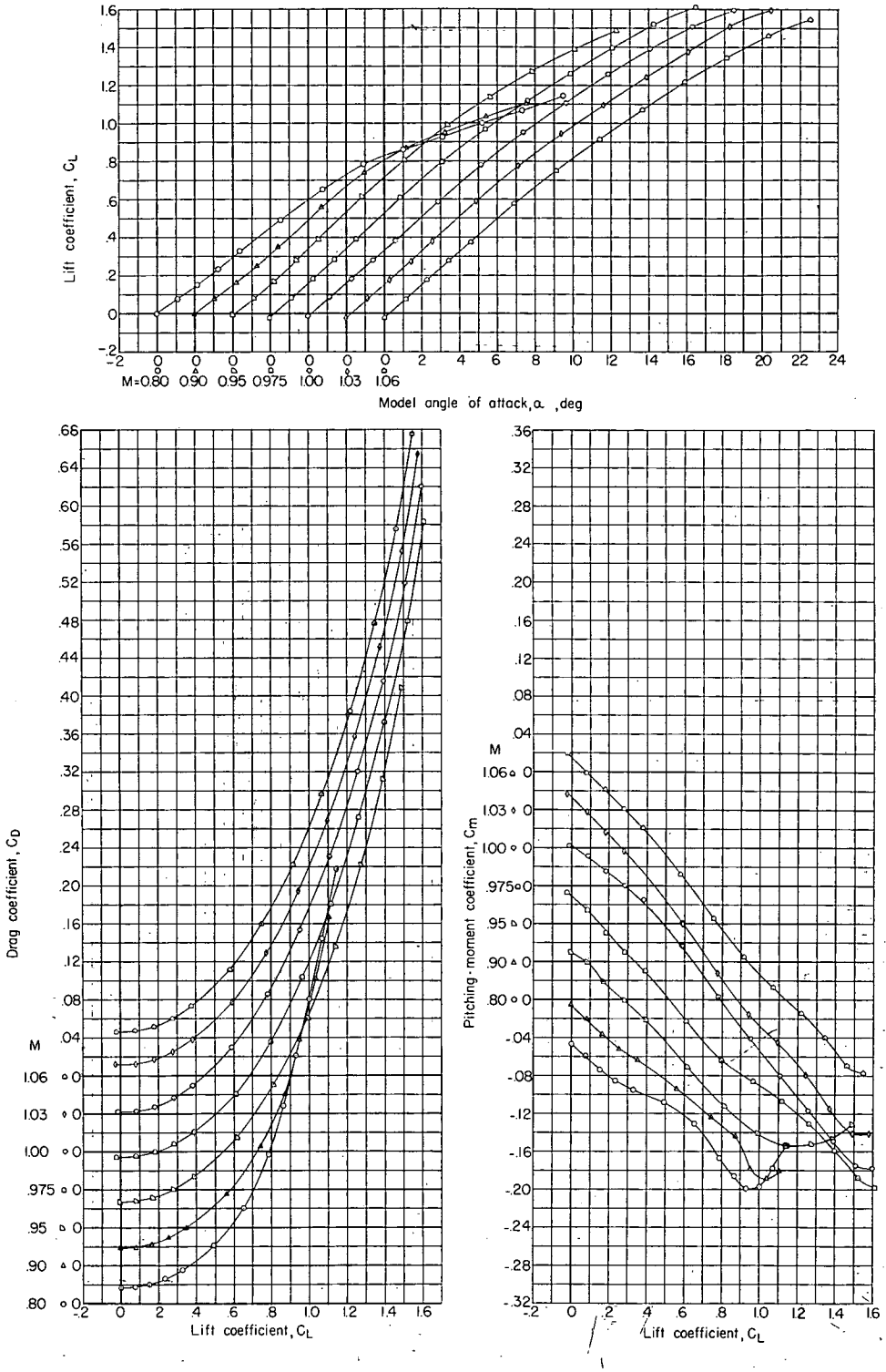

Figure 19.- Lift, drag, and pitching-moment characteristics. $WNFVH_{+4}H_A$ configuration.

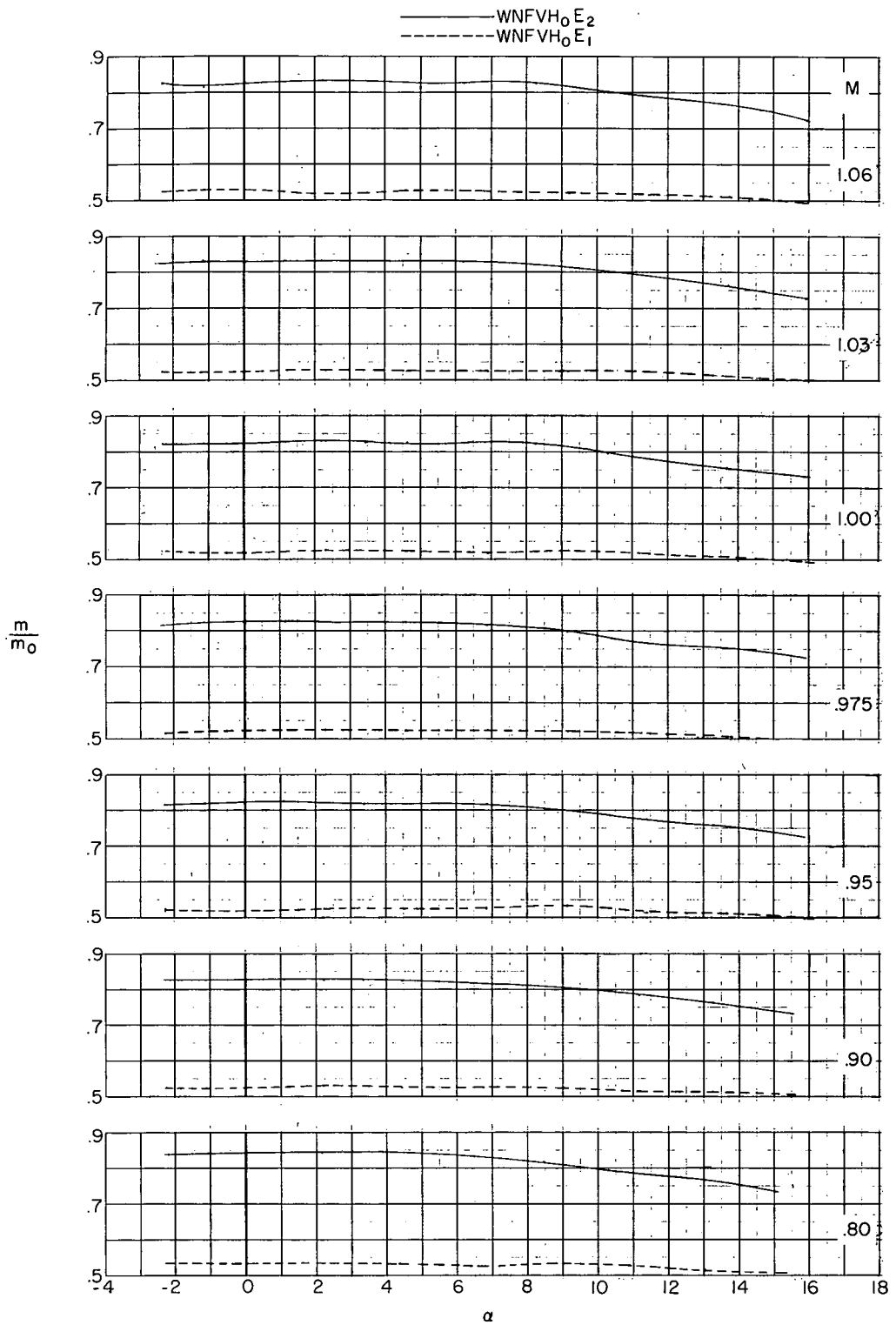

Figure 20.- Variation of mass-flow ratio with angle of attack and Mach number for the high and low mass-flow configurations.

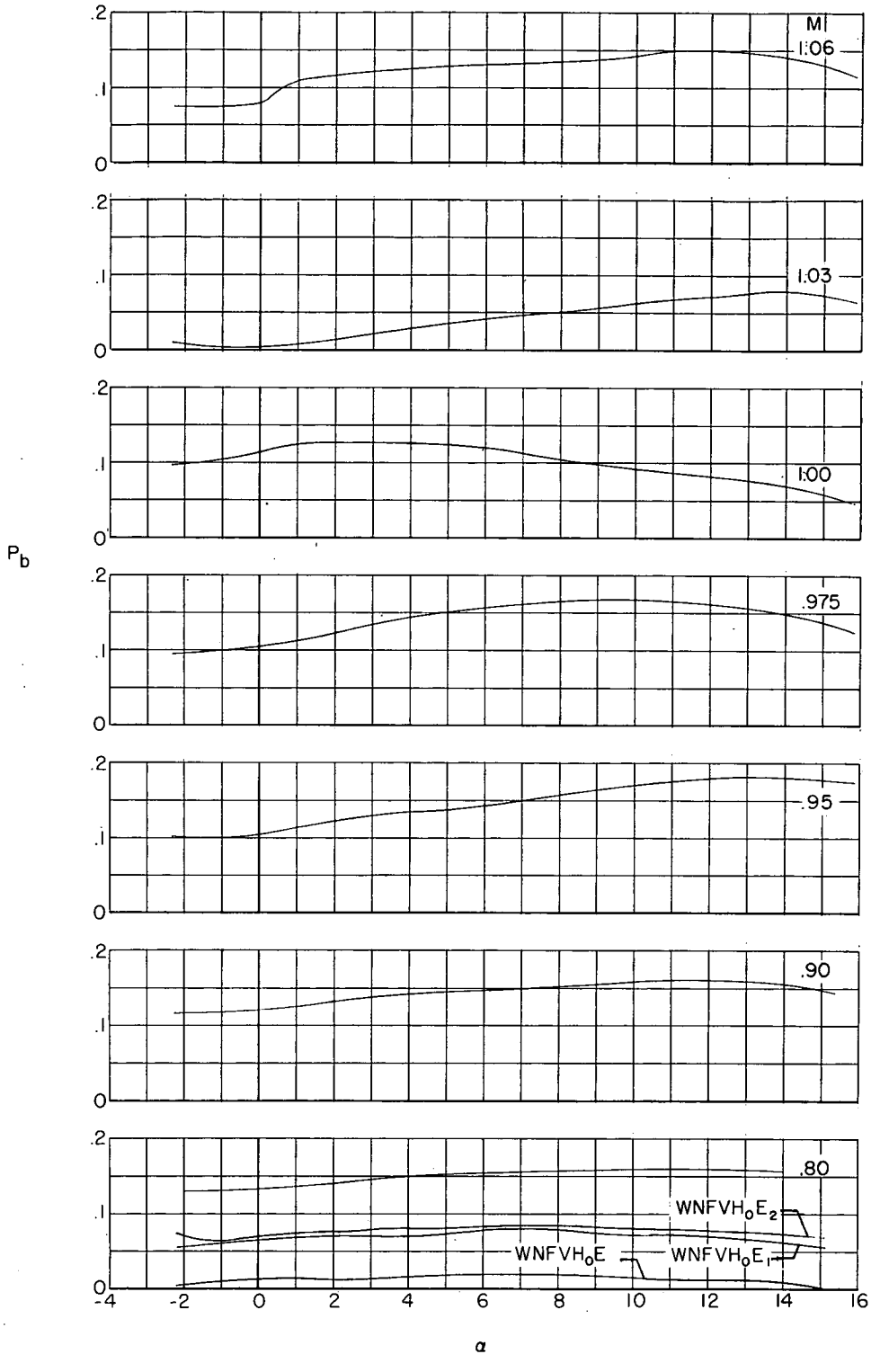

Figure 21.- Variation of base pressure coefficient with angle of attack and Mach number. WNFVH$_0$ configuration except where noted.

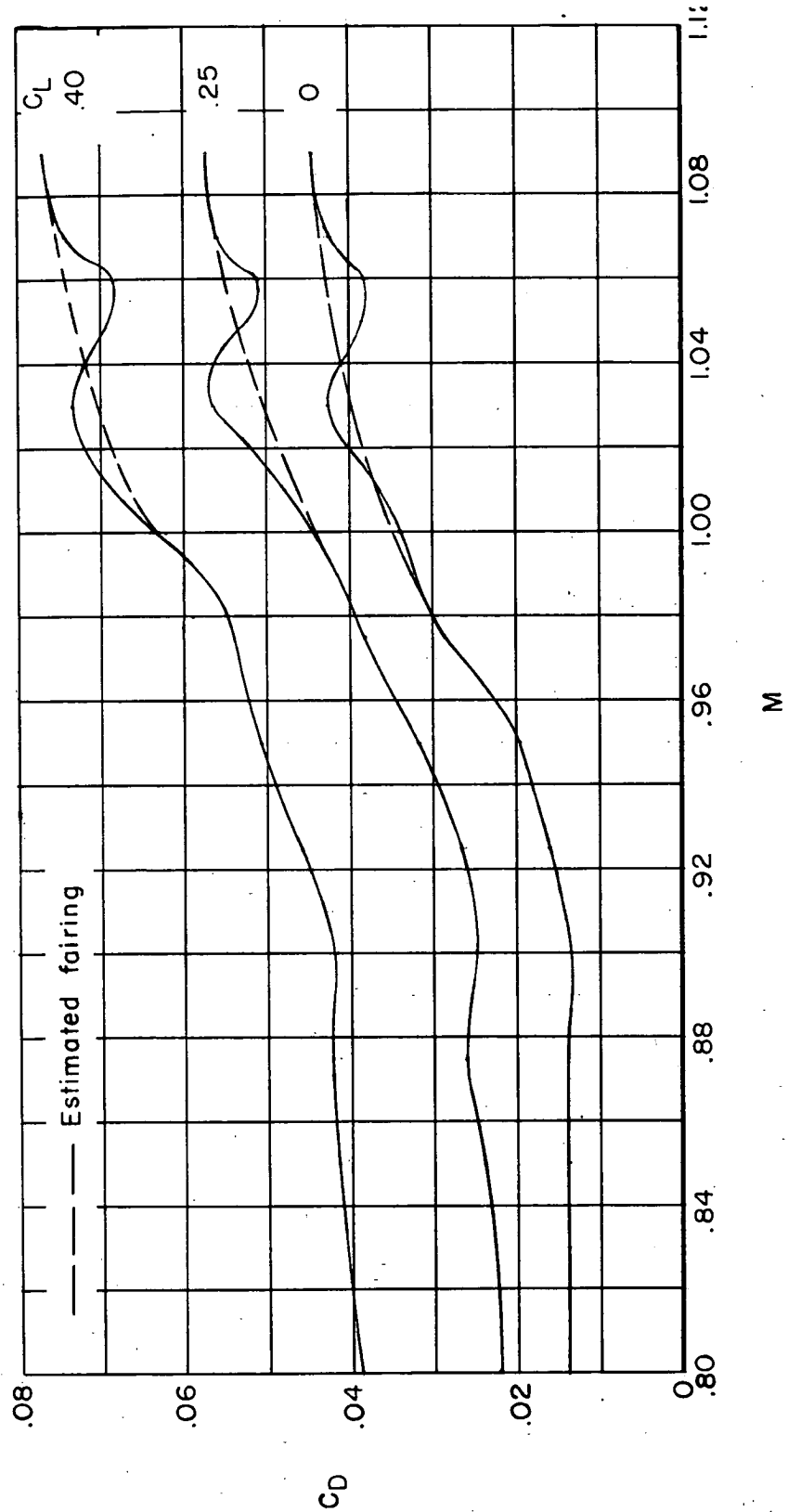

Figure 22.- Variation of drag coefficient with Mach number. $WNFVH_0E_2$ configuration. Data corrected for effect of modified afterbody.

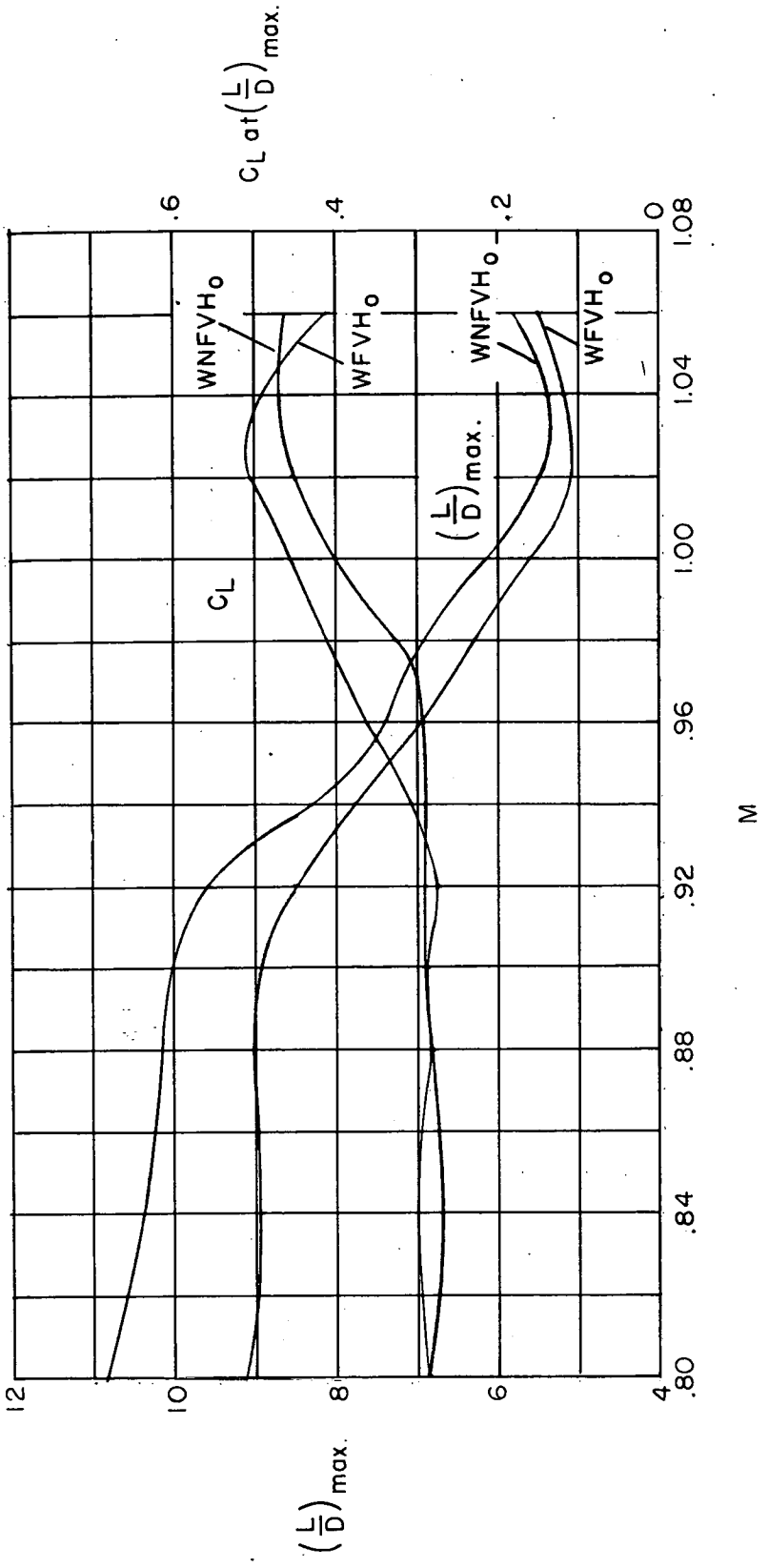

Figure 23.- Effect of drooped leading edge on maximum lift-drag ratio.

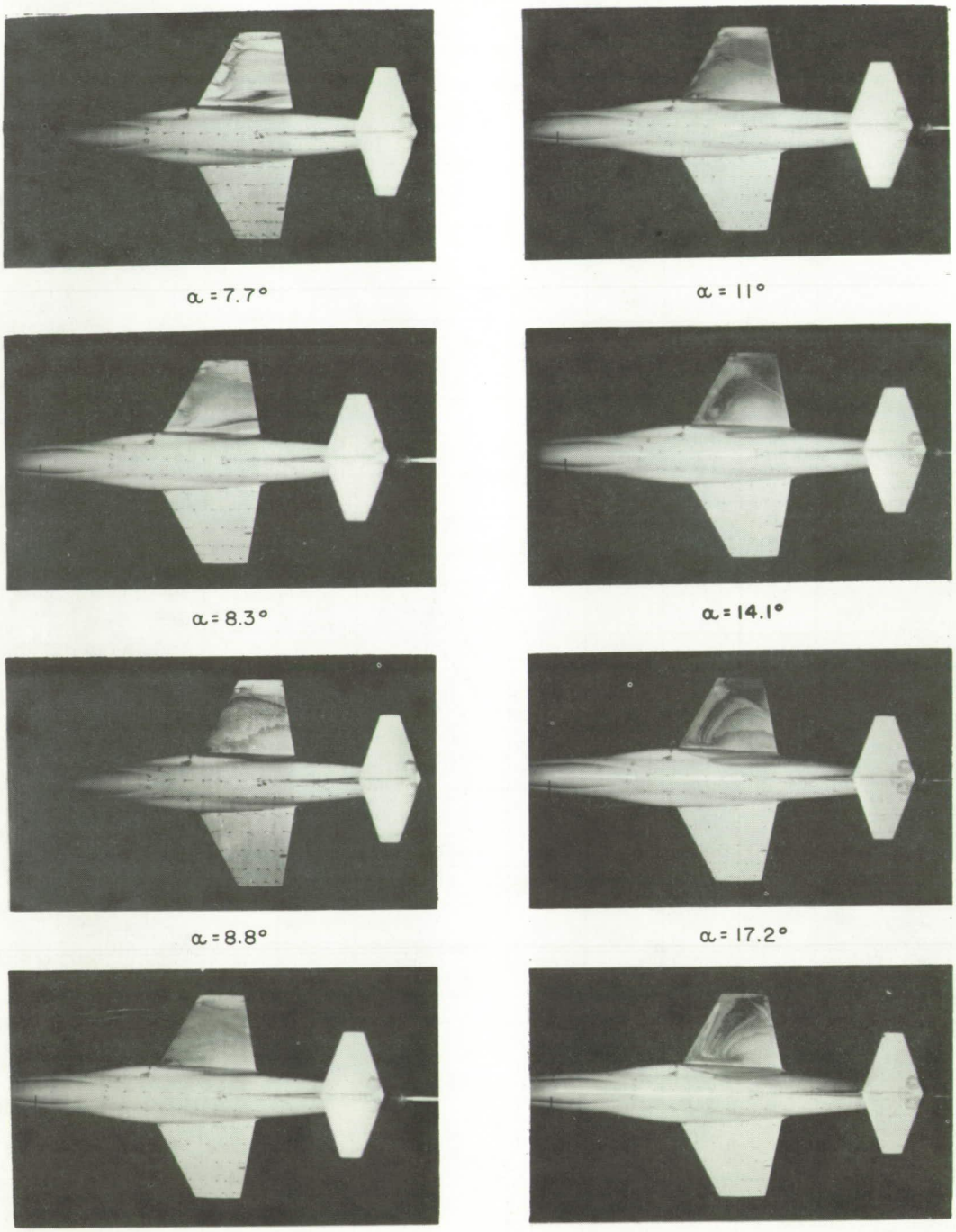

L-86485

(a) M = 0.80.

Figure 24.- Photographs of model showing tufts and liquid-film flow.

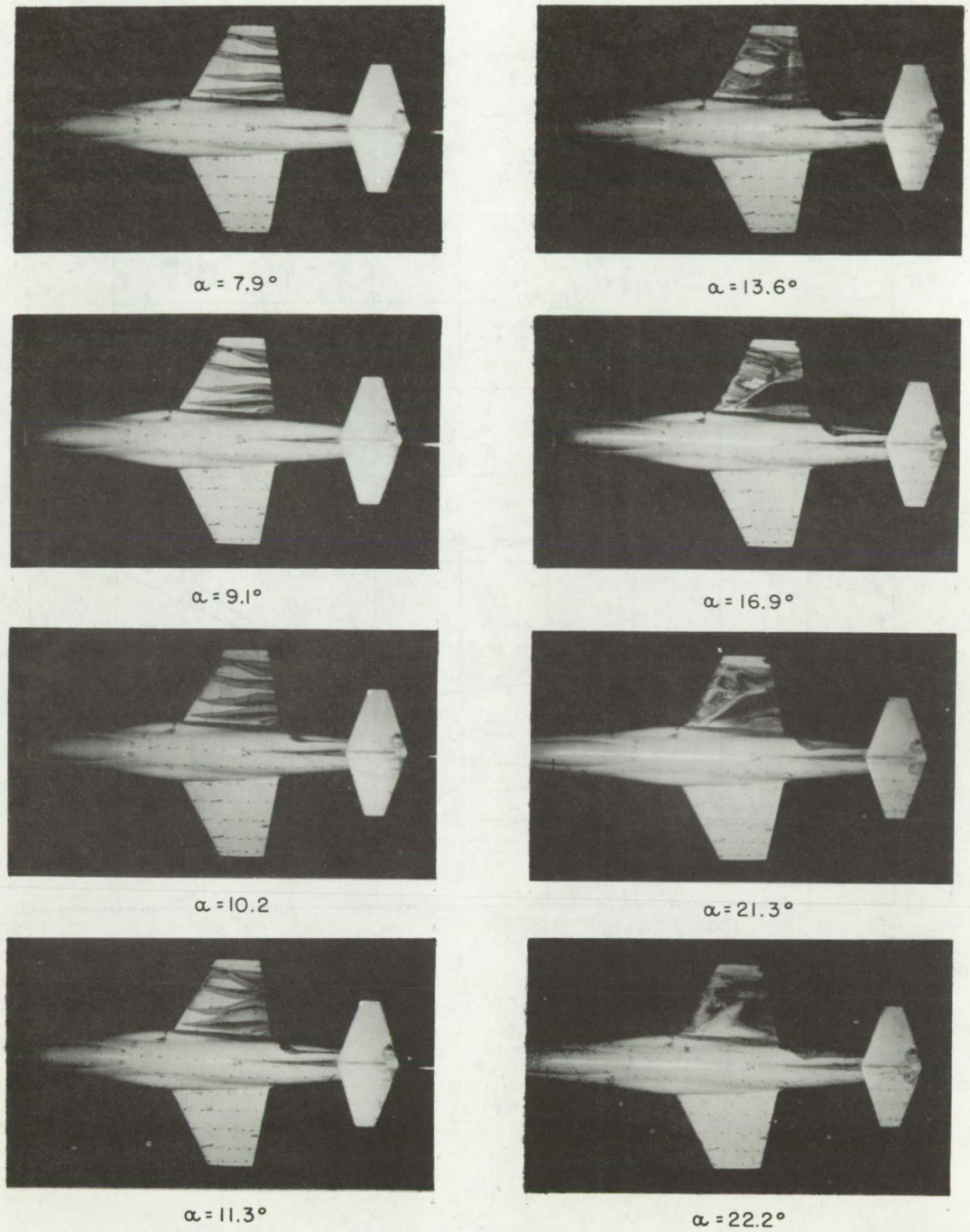

(b) M = 1.00.

L-86486

Figure 24.- Concluded.

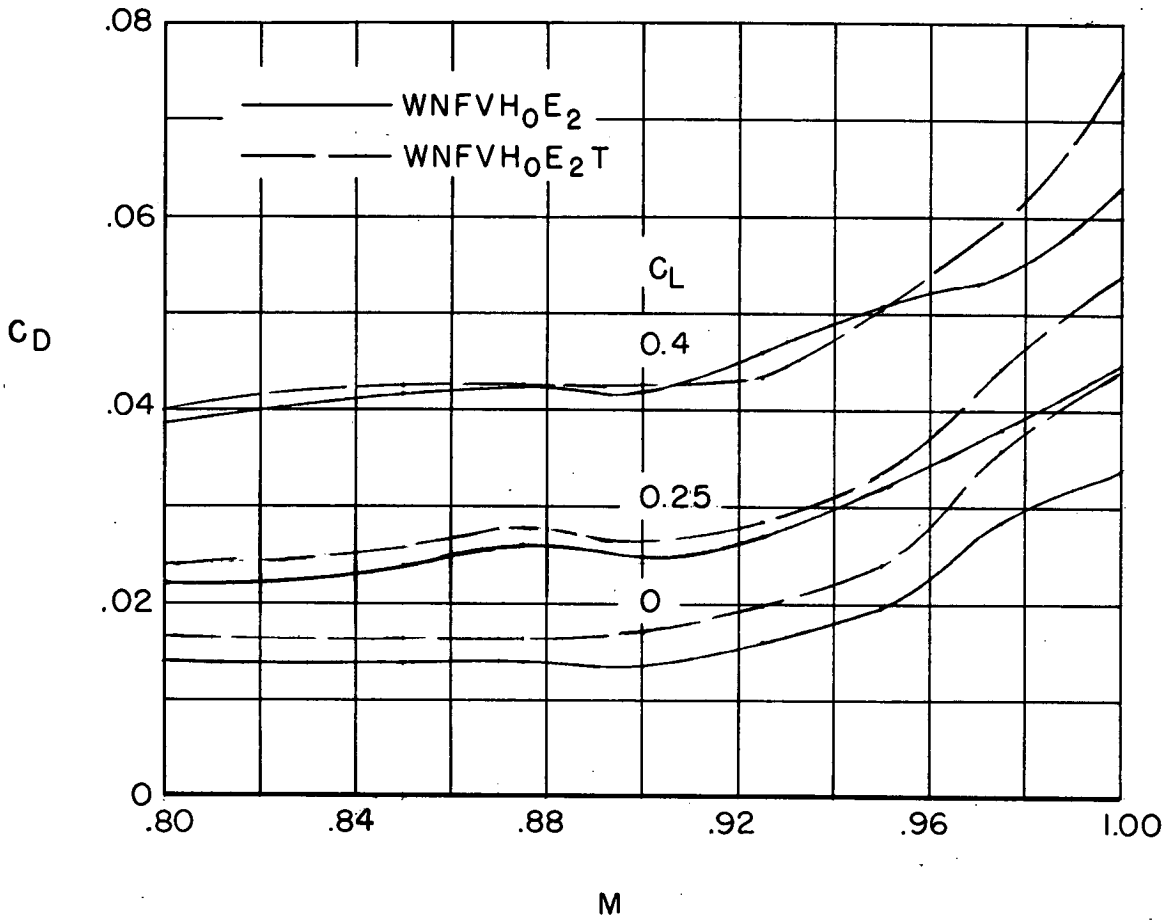

Figure 25.- Effect of tip tanks on drag coefficient. Data corrected for effect of modified afterbody.

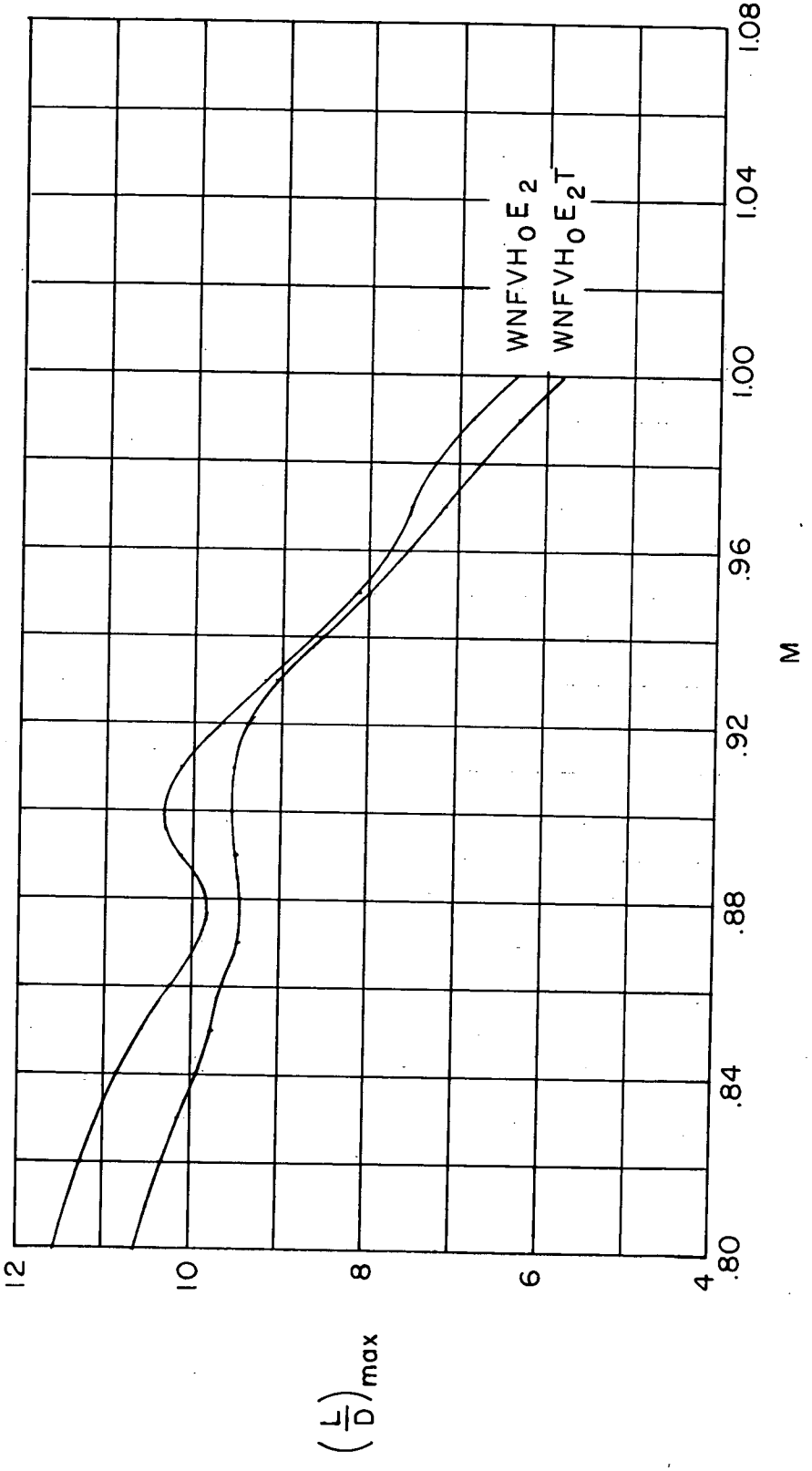

Figure 26.- Effect of tip tanks on maximum lift-drag ratio. Data corrected for effect of modified afterbody.

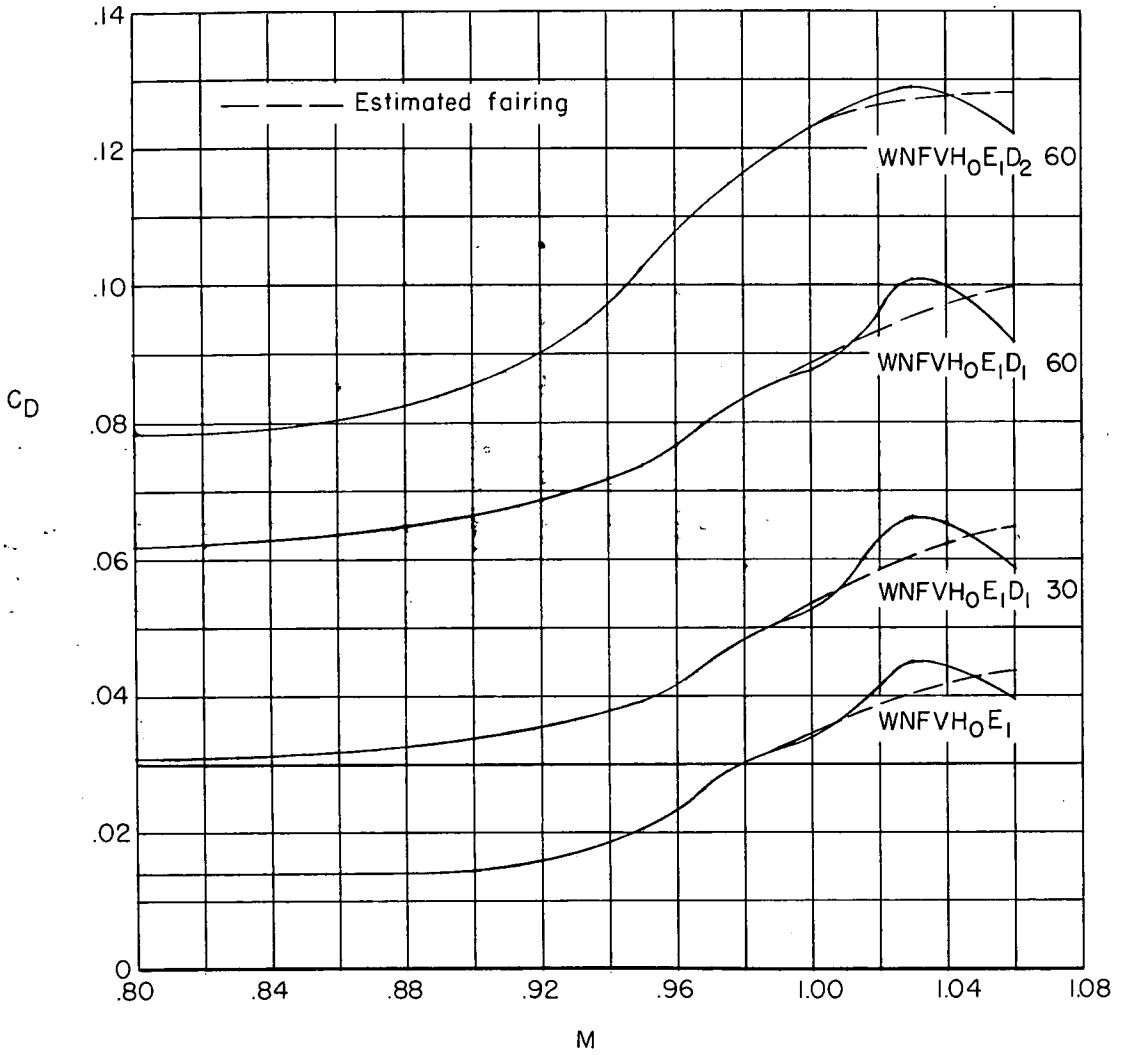

Figure 27.- Effect of dive flaps on model drag coefficient at zero lift. Data corrected for effect of modified afterbody.

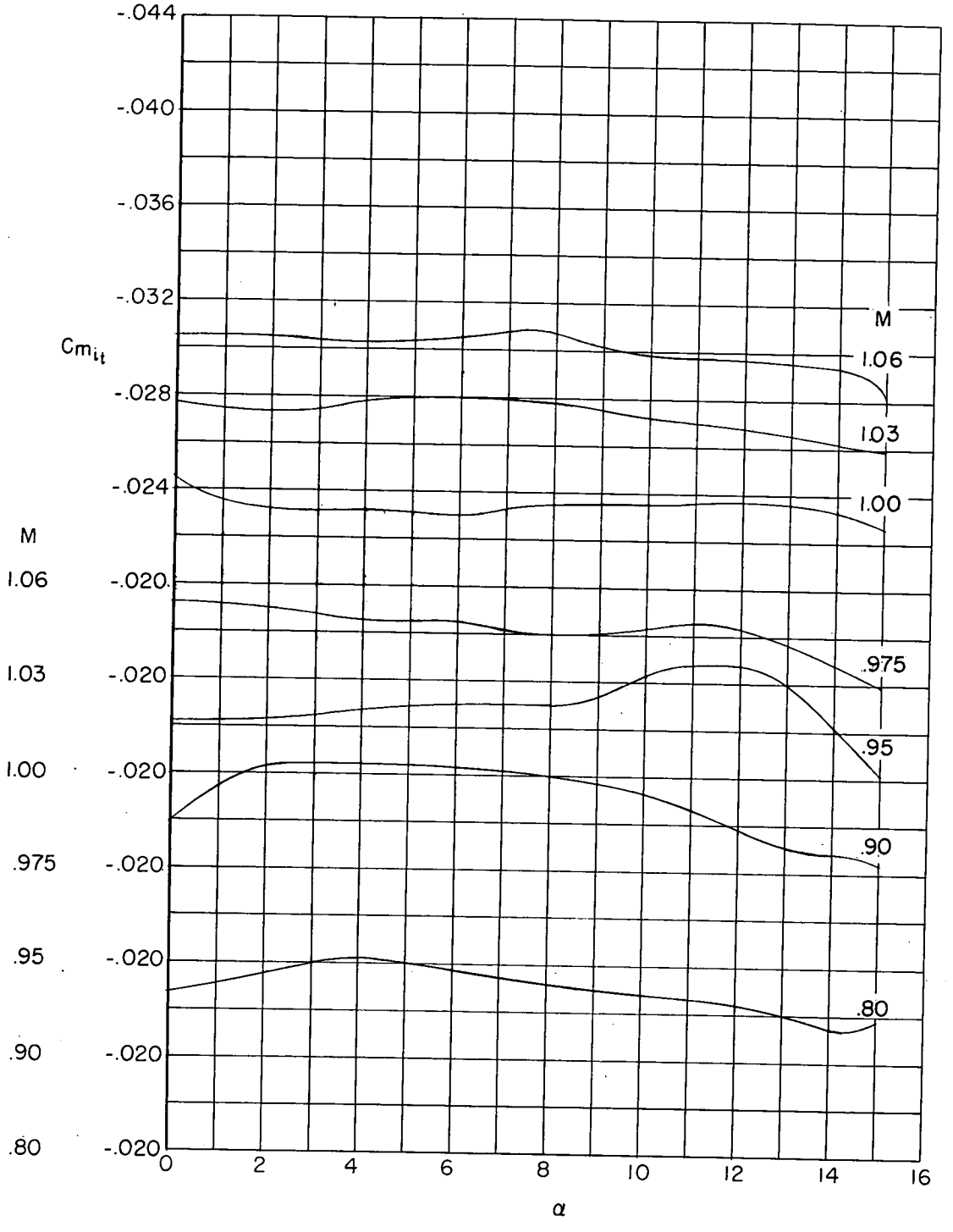

Figure 28.- Effect of angle of attack and Mach number on tail-effectiveness parameter $C_{m_{i_t}}$ for the configuration $WNFVHE_2$. Data not corrected for effect of modified afterbody.

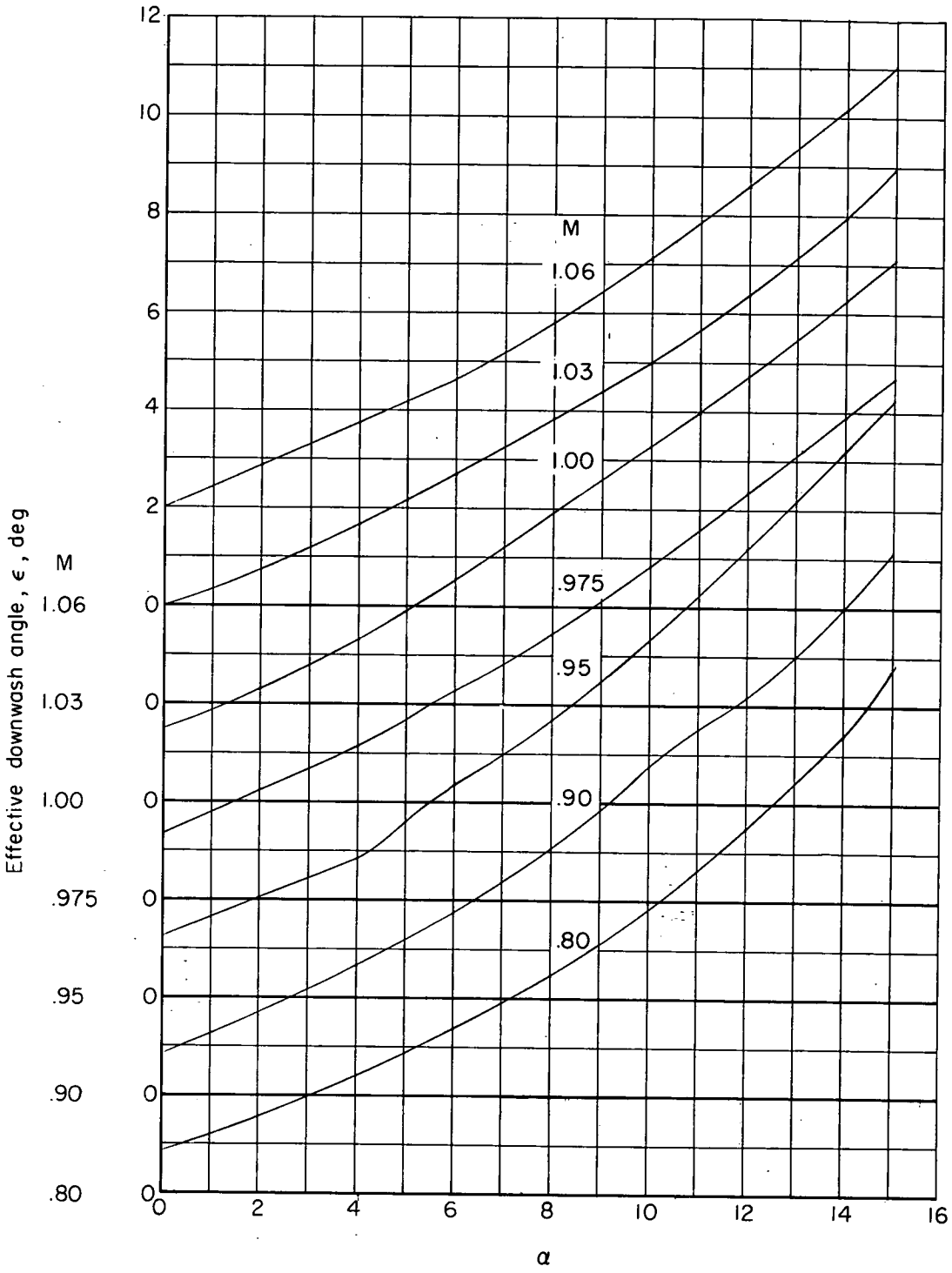

Figure 29.- Effect of angle of attack and Mach number on effective downwash angle. $WNFVHE_2$ configuration. Data not corrected for effect of modified afterbody.

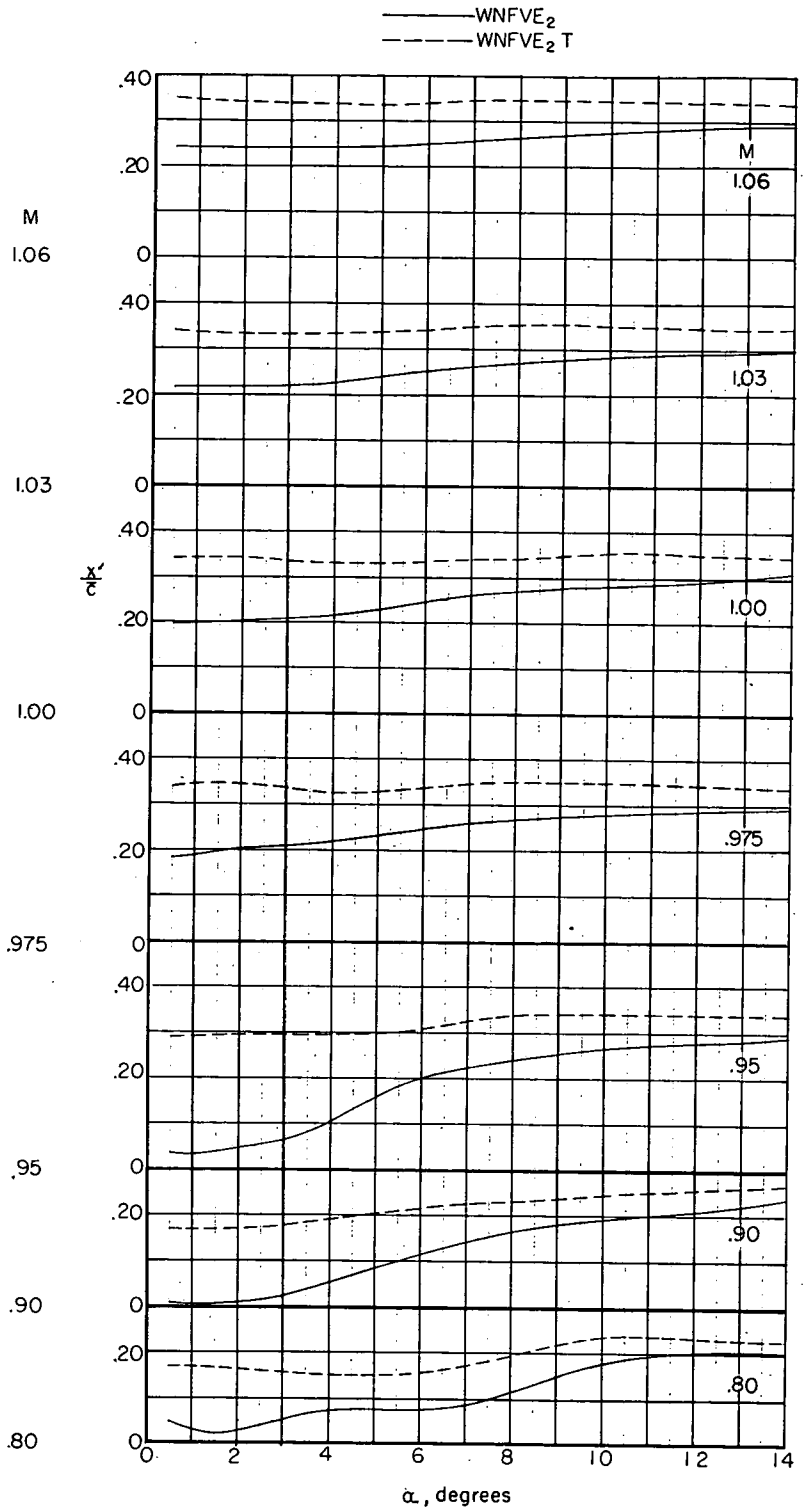

Figure 30.- Effect of tip tanks on chordwise center of normal load. Data not corrected for effect of modified afterbody.

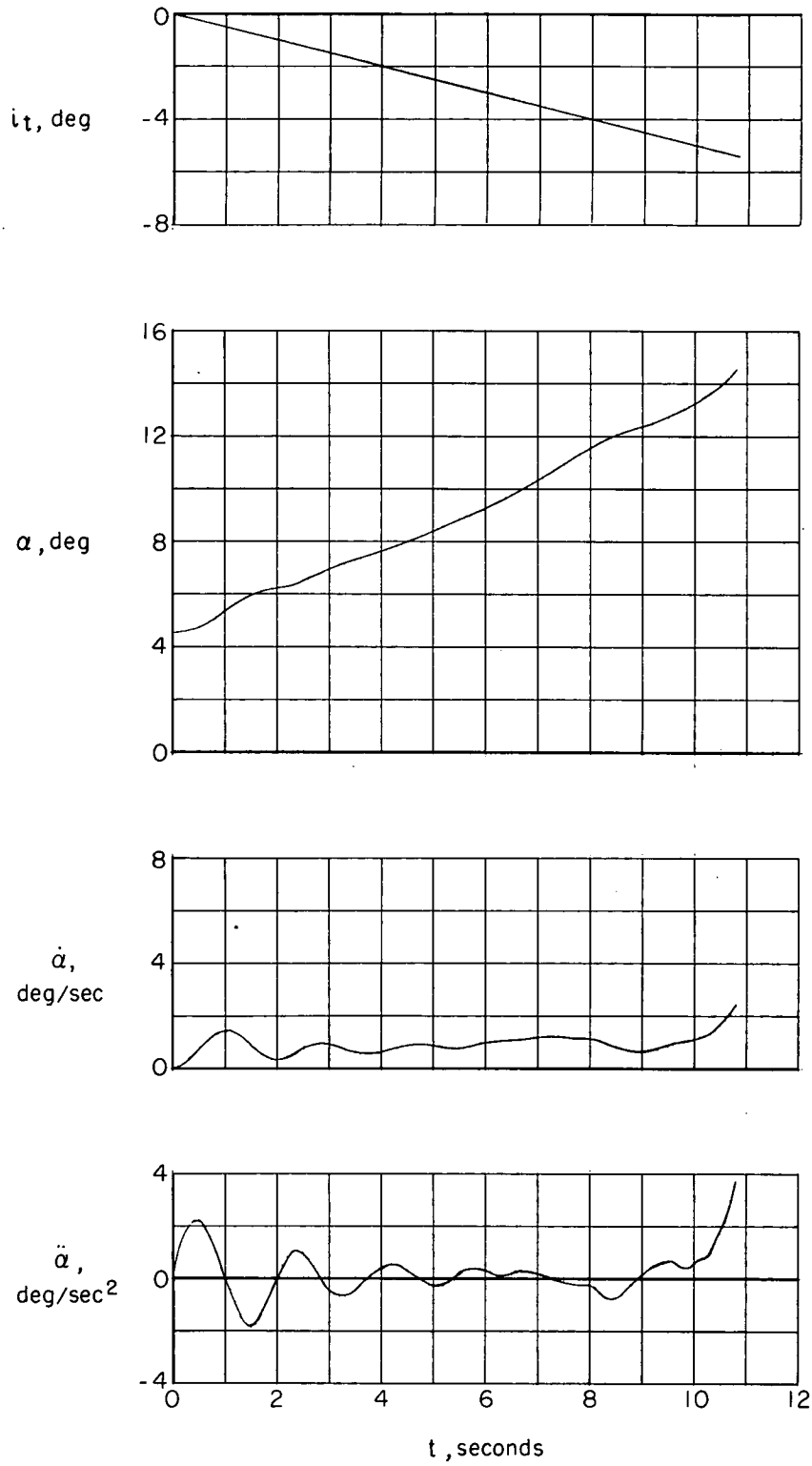

Figure 31.- Time response to a continuous variation of tail input of -0.5° per second. Mach number, 0.90; altitude, 40,000 feet.

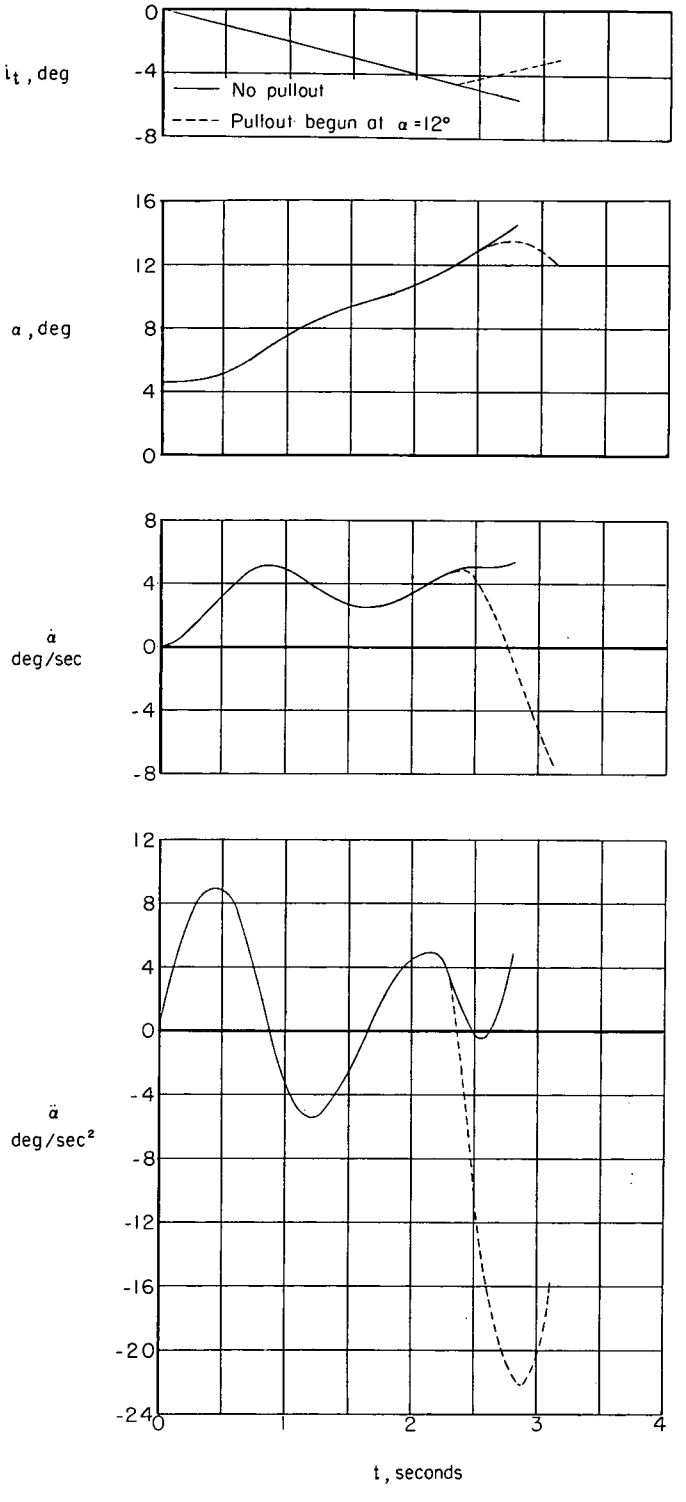

Figure 32.- Time response to a continuous variation of tail input of -2° per second and to a corrective tail input of 2° per second applied at $\alpha = 12^{\circ}$. Mach number, 0.90; altitude, 40,000 feet.

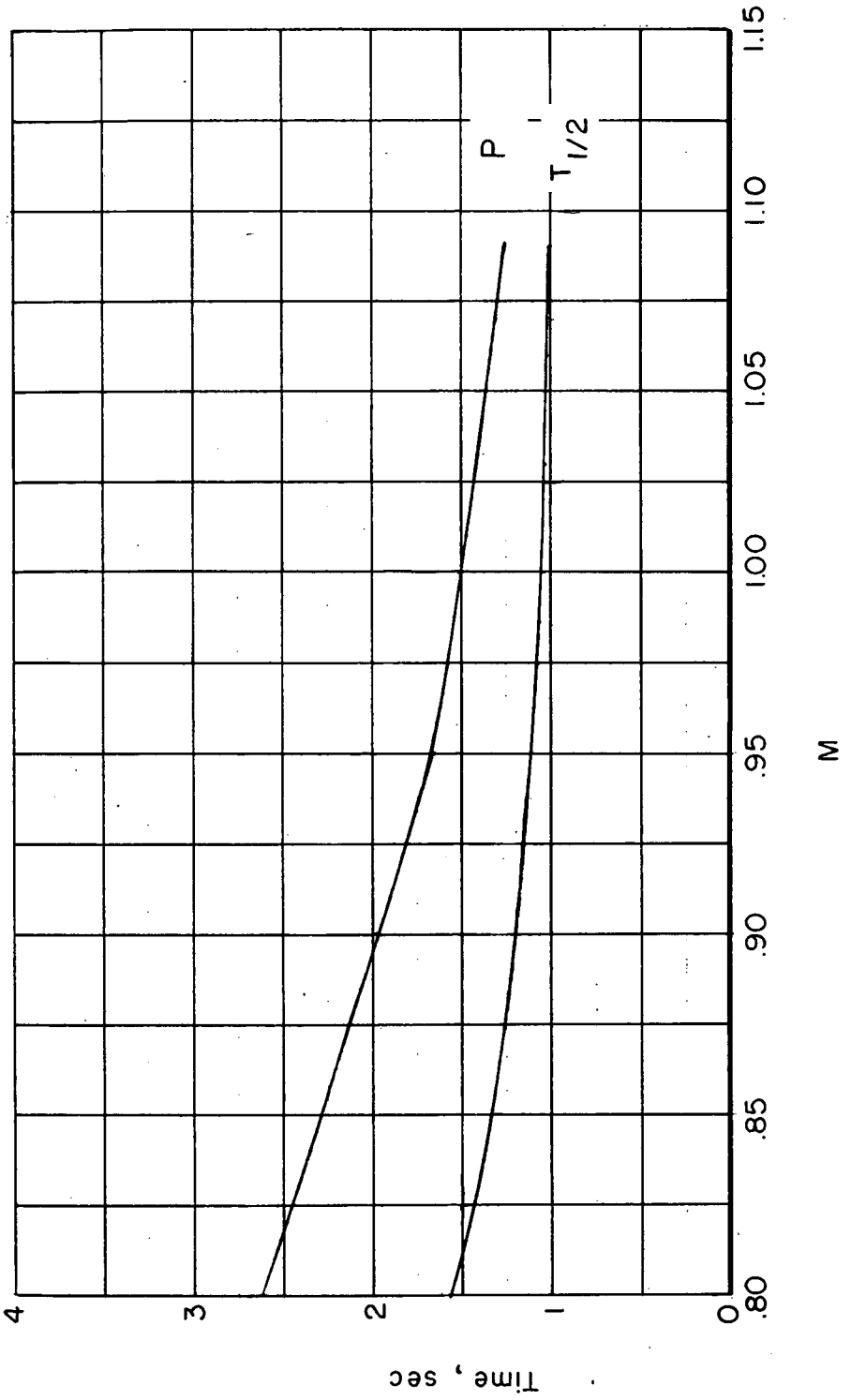

Figure 33.- Variation with Mach number of the period and time to damp to 1/2 amplitude of the short-period stick-fixed oscillations. Altitude, 40,000 feet.